Theoretical estimates of equilibrium carbon and hydrogen isotope effects in microbial methane production and anaerobic oxidation of methane

Jonathan Gropp[1,*], Mark A. Iron[2], and Itay Halevy[1]

[1]*Department of Earth and Planetary Sciences, Weizmann Institute of Science, Rehovot 7610001, Israel*

[2]*Computational Chemistry Unit, Department of Chemical Research Support, Weizmann Institute of Science, Rehovot 7610001, Israel*

[*]*Corresponding author, E-mail address: jonathan.gropp@weizmann.ac.il (J. Gropp)*

Abstract

Microbial production and consumption of methane are widespread in natural and artificial environments, with important economic and climatic implications. Attempts to use the isotopic composition of methane to constrain its sources are complicated by incomplete understanding of the mechanisms of variation in methane's isotopic composition. Knowledge of the equilibrium isotope fractionations among the large organic intracellular intermediates in the microbial pathways of methane production and consumption must form the basis of any exploration of the mechanisms of isotopic variation, but estimates of these equilibrium isotope fractionations are currently unavailable. To address this gap, we calculated the equilibrium isotopic fractionation of carbon ($^{13}C/^{12}C$) and hydrogen (D/H) isotopes among compounds in anaerobic methane metabolisms, as well as the abundance of multiple isotope substitutions ("clumping," e.g., ^{13}C–D) in these compounds. The Density Functional Theory calculations employed the M06-L/def2-TZVP level of theory and the SMD implicit solvation model, which we have recently optimized for large organic molecules and tested against measured equilibrium isotope fractionations. The computed $^{13}\beta$ and $^{2}\beta$ values decrease with decreasing average oxidation state of the carbon atom in the molecules, resulting in a preference for enrichment of the molecules with more oxidized carbon in ^{13}C and D. Using the computed β values, we calculated the equilibrium isotope fractionation factors in the prominent methanogenesis pathways (hydrogenotrophic, methylotrophic and acetoclastic) and in the pathway for anaerobic oxidation of methane (AOM) over a temperature range of 0-700 °C. Our calculated equilibrium fractionation factors compare favorably with experimental constrains, where available, and we used them to investigate the relation between the apparent isotope fractionation during

methanogenesis and AOM and the thermodynamic drive for these reactions. We show that a detailed map of the equilibrium fractionation factors along these metabolic pathways allows an evaluation of the contribution of equilibrium and kinetic isotope effects to apparent isotope fractionations observed in laboratory, natural and artificial settings. The comprehensive set of equilibrium isotope fractionation factors calculated in this study provides a firm basis for future explorations of isotope effects in methane metabolism.

1 INTRODUCTION

1.1 General

The isotopic distributions in thermodynamic equilibrium can be predicted with quantum mechanical calculations. These theoretical predictions are invaluable in exploring isotope fractionation systematics where experimental data are lacking or hard to obtain (e.g., Rustad et al., 2008; Eldridge et al., 2016), such as for the intracellular components of biological production and oxidation of methane (methanogenesis and methanotrophy, respectively). Theoretical approaches, in particular density functional theory (DFT), have been widely applied to small molecules (Li & Liu, 2011; Fujii et al., 2014), and recently also to large organic molecules (Black et al., 2007; Rustad, 2009; Wang et al., 2009a,b, 2013; Moynier & Fujii, 2017; Iron & Gropp, 2019) in the gas, aqueous and solid phases. The application of DFT is of special interest in methanogenesis and methanotrophy since these processes involve large organic molecules, which have received less attention than small molecules due to issues of calculation cost and accuracy (Iron & Gropp, 2019). Consequently, studies to date of the isotopic compositions in methanogenesis and methanotrophy have focused on the extracellular substrates and products, mainly H_2, CO_2, CH_4 and H_2O, but have neglected the intracellular components of these processes. To bridge this gap, we (*i*) provide a novel set of constraints on the temperature-dependent carbon and hydrogen isotope equilibrium fractionation factors (EFFs) among the intracellular molecules involved in the methanogenesis and methanotrophy pathways, (*ii*) compare these results to previous reports, mostly of the pathway end-members, and (*iii*) discuss the possible application and the associated caveats of these results in geochemical and bioisotopic models.

1.2 Methanogenesis and anaerobic methanotrophy

1.2.1 Physiology of methanogens and methanotrophs

Methanogenic organisms produce methane by fixing CO_2 in the hydrogenotrophic pathway or by reducing methylated compounds, such as acetate (i.e., acetoclastic methanogenesis) or methanol (i.e., methylotrophic methanogenesis), as described in the following net reactions:

$$CO_2 + 4H_2 \rightleftarrows CH_4 + 2H_2O\,, \tag{1}$$

$$CH_3COOH \rightleftarrows CH_4 + CO_2\,, \tag{2}$$

$$4CH_3OH \rightleftarrows 3CH_4 + CO_2 + 2H_2O\,. \tag{3}$$

These three metabolic pathways have been described in detail (Thauer et al., 2008), and all are assumed to originate from a single, common ancestor that utilized a version of the hydrogenotrophic pathway (Berghuis et al., 2019) (Fig. 1). In the hydrogenotrophic pathway (Eq. 1), CO_2 is reduced

to methane in seven, consecutive enzymatic reactions, with four reduction steps, which are mediated by the electron carriers ferredoxin (Fd), coenzyme F_{420} (F_{420}) and coenzyme B (HS-CoB). In acetoclastic methanogenesis (Eq. 2), acetate (CH_3COO^-) is initially activated to acetyl-CoA (CH_3-COSCoA). The methyl group is then transferred to tetrahydromethanopterin (H_4MPT) and then into the classic hydrogenotrophic pathway (Welte & Deppenmeier, 2014), while the CoA-bound carbonyl carbon is oxidized to CO_2. In the methylotrophic pathway (Eq. 3), the methyl group is transferred from methanol directly to HS-CoM to form methyl coenzyme M (CH_3-SCoM). The CH_3-SCoM then disproportionates to either CO_2 in the oxidative reverse-methanogenesis pathway or to methane in the reductive pathway. The reductive and oxidative branches of this pathway operate at a ratio of $\sim$3:1, to balance the electrons needed for the reduction of CH_3-SCoM (Vanwonterghem et al., 2016).

Anaerobic oxidation of methane (AOM) is an important process in mitigating the emission of methane from anoxic sediments to the atmosphere (Egger et al., 2018). More specifically, AOM is mediated by anaerobic methanotrophs (ANME) in a modified reverse-methanogenesis pathway, where the same enzymes of the hydrogenotrophic pathway catalyze methane oxidation. The oxidation is generally coupled to syntrophic sulfate, nitrate or ferric iron reduction (Scheller et al., 2010; Thauer, 2011; McGlynn, 2017; Scheller et al., 2017).

1.2.2 Isotopic composition of methane

The hydrogen (D/H) and carbon ($^{13}C/^{12}C$) isotope ratios of methane have been extensively used to distinguish among environmental methane sources (Whiticar, 1999), yet the sources often overlap in their characteristic isotopic compositions (e.g., Alstad & Whiticar, 2011), masking the source of methane. Recent developments in the precise measurement of the abundance of the doubly-substituted ("clumped") isotopologues of methane (i.e., $^{13}CH_3D$ and $^{12}CH_2D_2$) further constrain the temperature of methane formation under equilibrium conditions (Stolper et al., 2014; Ono et al., 2014; Stolper et al., 2015). However, disequilibrium clumped isotope compositions are common in laboratory and natural settings (Wang et al., 2015; Gruen et al., 2018; Young, 2019), and the mechanisms that control these departures from equilibrium are incompletely understood.

Bioisotopic models have the potential to reveal details of the elusive mechanisms that control such isotopic fingerprints. Such models have been successfully applied to microbial sulfate reduction by demonstrating how the sulfur isotope fractionations of individual steps in the pathway combine to control the net fractionation (Wing & Halevy, 2014; Zaarur et al., 2017; Wenk et al., 2017). Previous application of simplified isotope mass-balance models to the hydrogenotrophic methanogenesis pathway assign EFFs of the intracellular intermediate reactions as free parameters without any theoretical or experimental constraints (Wang et al., 2015; Stolper et al., 2015; Cao et al., 2019). To address this gap, to facilitate the application of bioisotopic models to microbial production and consumption of methane, and to allow a better understanding of data from laboratory experiments

and natural environments, we provide hydrogen and carbon isotope and clumped isotopologue EFF values for the three main pathways of methanogenesis and for 'reverse-methanogenesis' AOM.

1.3 Calculating equilibrium fractionation factors

Experimentally-measured EFFs are the basis for understanding the distributions of isotopes in many geochemical systems, but the scope of these methods is often limited by long equilibration times at low temperatures, potential fractionation during the sampling processes, and complex separation procedures of the reactants and products. Early studies demonstrated that EFFs can be calculated from the observed molecular vibrational frequencies using a simplified quantum mechanical model of the experimentally measured molecular vibrations and rotations and expressed as a reduced partition function ratio (RPFR) (Urey, 1947; Bigeleisen & Mayer, 1947). Subsequently, computational methods such as Hartree–Fock (HF) (Roothaan, 1951) and DFT (Hohenberg & Kohn, 1964; Kohn & Sham, 1965) provided an independent means of estimating the vibrational frequencies. These approaches have been extensively used to study several systems of geochemical interest, primarily for small molecules in the gaseous and aqueous phases, including sulfur compounds (Otake et al., 2008; Eldridge et al., 2016), metals (Domagal-Goldman & Kubicki, 2008; Fujii et al., 2014) and crystalline solids (e.g., Méheut et al., 2007). Application to large organic molecules in the aqueous phase has remained limited due to computational cost and inaccurate results. Accordingly, in methanogenesis, experimental and theoretical work so far has focused on the small gaseous end-members, namely the H_2O–H_2, CH_4–H_2 and CO_2–CH_4 systems (e.g., Suess, 1949; Bottinga, 1969; Horibe & Craig, 1995; Horita, 2001), and not on the intracellular organic intermediates.

There have been attempts to calculate EFFs among large organic molecules for some elements, such as Mg (Black et al., 2007; Moynier & Fujii, 2017), C (Rustad, 2009), Cu (Tennant et al., 2017) and H (Wang et al., 2009a,b, 2013). Wang et al. (2009a; 2013) compared experimental and DFT calculations (B3LYP/6-311G**) of hydrogen isotope EFFs of the C_α positions in ketones finding a good overall agreement. The B3LYP functional is commonly used in geochemical DFT calculations, and is the most commonly used functional in general. However, there are more modern and cost-effective methods, such as M06-L (Zhao et al., 2006) or HCTH/407 (Boese & Handy, 2001), and until recently the accuracy of these and other functionals in predicting EFFs of large organic molecules has not been systematically compared. We recently conducted a thorough examination of various DFT functionals and basis sets to determine the uncertainty associated with the prediction of EFFs of H, C, N and O stable isotopes among large soluble organic molecules (Iron & Gropp, 2019). The mean unsigned error (MUE) of these calculations in predicting the hydrogen fractionation in the C_α position of linear and cyclic ketones is 20.8‰, comparable to the results of Wang et al. (2009a; 2013). For C, N and O isotopes, there was an insignificant difference between the various methods, but the M06-L functional with the def2-TZVP basis set and the SMD solvation model yielded the best fits, with an MUE of 2.3‰ for carbon isotopes. In this study, we employed

the best-fit DFT model (M06-L functional, def2-TZVP basis set, SMD solvation model) to calculate a novel set of carbon and hydrogen equilibrium fractionation factors for the species involved in the core methanogenesis and AOM pathways. This dataset can aid in the interpretation of isotopic fractionations during methanogenesis and methanotrophy, in both laboratory cultures and natural environments. Moreover, this dataset eliminates a degree of freedom from future bioisotopic models, which could potentially be used to understand disequilibrium methane isotope compositions and their physiological and environmental implications. We will discuss the uncertainties in our predictions and their implications for the observations of the isotopic composition of methane in various systems.

2 METHODS

2.1 Overview: the Bigeleisen–Mayer equation

The RPFR is the equilibrium fractionation factor of a given isotope pair in a given molecule:

$$\mathrm{RPFR} = \frac{\sigma}{\sigma^*} \prod_{i=1}^{3N-6(5)} \frac{u_i^*}{u_i} \cdot \frac{\exp(-u_i^*/2)}{\exp(-u_i/2)} \cdot \frac{1-\exp(-u_i)}{1-\exp(-u_i^*)} \tag{4}$$

where $u_i = hc\omega_i/k_B\mathrm{T}$, h is the Planck constant, c is the speed of light, ω_i are the vibrational frequencies, k_B is the Boltzmann constant, T is the absolute temperature, σ is the symmetry number (most large organic molecules lack any symmetry so this term is often unity), and the asterisk denotes the species with the heavy isotope(s). The product runs over the $3N-5$ or $3N-6$ vibrational frequencies of linear and non-linear molecules, respectively, where N is the number of atoms in the molecule. The three ratios in the product are the classical factor accounting for rotational and translational energy, the zero-point energy (ZPE) contribution, and the excitation factor. The RPFR can be directly related to the β factor, which is the RPFR of a compound and an ideal monoatomic gas. For single isotope substitutions, when the excess factors are ignored, β = RPFR, and the (temperature-dependent) EFF between two species (α) that contain the rare isotope r is the ratio of the respective βs: ${}^{r}\alpha^{\mathrm{eq}}_{\mathrm{A-B}} = {}^{r}\beta_{\mathrm{A}}/{}^{r}\beta_{\mathrm{B}}$.

We also calculated the EFFs of doubly-substituted (clumped) isotopologues that contain a single ^{13}C–D bond. The abundance of clumped isotopologues is commonly reported as the deviation from the expected stochastic distribution, $\Delta_i^{\mathrm{eq}} \equiv \left(R_i^{\mathrm{eq}}/R_i^* - 1\right)$ where i is the isotopologue of interest, R_i^{eq} is the abundance of the clumped isotopologue relative to the nonsubstituted isotopologue at equilibrium, and R_i^* is its abundance at a stochastic distribution of the rare isotopes. We calculated Δ_i^{eq} from RPFRs following Cao and Liu (2012), who suggested that Δ_i^{eq} of the clumped isotopologue $\mathrm{V'Y'Y}_{n-1}$, where V′ and Y′ are the rare isotopes of atoms V and Y, respectively, and n is the number of Y atoms in the molecule VY_n, can be calculated by the general relation:

$$\Delta_{\mathrm{V'Y'Y}_{n-1}} = \left(\frac{(\sigma^*/\sigma) \times {}^{\mathrm{V'Y'}}\mathrm{RPFR}_{\mathrm{VY}_n}}{{}^{\mathrm{V'}}\beta_{\mathrm{VY}_n} \times {}^{\mathrm{Y'}}\beta_{\mathrm{VY}_n}} \right) \tag{5}$$

where ${}^{\mathrm{V'Y'}}\mathrm{RPFR}_{\mathrm{VY}_n}$ is the RPFR of the clumped isotopologue of interest. ${}^{\mathrm{V'}}\beta_{\mathrm{VY}_n}$ and ${}^{\mathrm{Y'}}\beta_{\mathrm{VY}_n}$ are approximately equal to the β values of single substitutions of V′ and Y′ in VY_n (Cao & Liu, 2012). In addition to the internal equilibrium distribution of V′–Y′ bonds in the molecule VY_n (Eq. 5), we are interested in the distribution of V′–Y′ bonds in large organic molecules of the general form $x\mathrm{VY}_n$, where x denotes an arbitrary molecular residue. We calculated the EFFs of reactions that include a clumped isotopologue and distinguish between primary isotope effects, where a new V′–Y′ bond is formed or broken:

$${}^{\mathrm{V'Y'}}\alpha_{a\mathrm{V'Y},b\mathrm{VY'}/c\mathrm{V'Y'}} = {}^{\mathrm{V'}}\beta_{a\mathrm{V'Y}} \times {}^{\mathrm{Y'}}\beta_{b\mathrm{VY'}}/{}^{\mathrm{V'Y'}}\mathrm{RPFR}_{c\mathrm{V'Y'}} \tag{6}$$

and secondary isotope effects, where an original V′–Y′ bond remains intact:

$$^{\mathrm{V'Y'}}\alpha_{a\mathrm{V'Y'}/c\mathrm{V'Y'}} = {}^{\mathrm{V'Y'}}\mathrm{RPFR}_{a\mathrm{V'Y'}} / {}^{\mathrm{V'Y'}}\mathrm{RPFR}_{c\mathrm{V'Y'}} \tag{7}$$

2.2 Quantum mechanical calculations of partition coefficients for large organic molecules

All calculations were done with GAUSSIAN16 revisions A.03, B.01 AND C.01 (Frisch et al., 2016). Based on its performance in predicting EFFs in large organic molecules (Iron & Gropp, 2019), we chose the M06-L DFT exchange–correlation functional and def2-TZVP basis set (Andrae et al., 1990; Kaupp et al., 1991; Leininger et al., 1996; Metz et al., 2000; Weigend & Ahlrichs, 2005). Vibrational frequencies were scaled prior to being used in the Bigeleisen–Mayer equation, using previously determined factors (λ_{harm} = 0.9965, λ_{ZPE} = 0.9825). This has been shown to provide a more accurate prediction of vibrational frequencies (Kesharwani et al., 2016). Separate scaling factors were used for the harmonic frequencies and zero-point (vibrational) energy terms in Eq. 4 (for further details, see Iron and Gropp, 2019).

The original derivation of RPFR by Bigeleisen and Mayer suited molecules in a gas phase, but biochemical reactions within the cells usually occur in the aqueous phase. Adding explicit water molecules should, in principle, yield more accurate results for reactions in aqueous solution, but this also increases the size of the system and associated calculation costs. Implicit solvation models, which assume that the solvent effects can be described by the free energy cost of solvation alone, thereby offering a substantial reduction in computational cost, are a common solution to this issue (Tomasi et al., 2005). We generated the RPFRs of the end-member molecules in both the gaseous and aqueous phases. To account for the aqueous phase, we used the SMD solvation model of Truhlar and coworkers (Marenich et al., 2009).

In this work, we use the singly substituted hydrogen isotopologues as a proxy for the bulk D/H ratios of the compounds, which is a common practice for isotopologues with atoms in equivalent positions (Galimov, 2006; Wang et al., 2009a; Liu et al., 2010). We perform our DFT calculations for frozen-geometry molecules, which produce distinct RPFR values for substitution of D for H in the different positions of the methyl groups. The free rotation of the methyl group makes the three C–H bonds equivalent and chemically indistinguishable, and we therefore calculate the RPFR of the deuterated molecule from the arithmetic mean of RPFR values determined from the distinct site-specific D/H-substitutions (Wang et al., 2009a).

Liu et al. (2010) considered a number of corrections to the Bigeleisen–Mayer equation, including anharmonic effects and vibrational–rotational couplings. However, they studied small, triatomic molecules, where these corrections are small. In our previous study, where we considered much larger molecules, it was found that these terms were actually detrimental to the accuracy of the results (Iron & Gropp, 2019). We hypothesized that the degradation of accuracy may result

from the inclusion of these terms violating the underlying assumptions of the Bigeleisen–Mayer equation, specifically, the assumptions of a rigid rotor and a harmonic oscillator, which in turn allow the use of the Teller–Redlich product rule.

He et al. (2019) recently suggested that truncating large organic molecules to ease the calculation cost may have a negligible effect on $^{13}\alpha$ predictions when used with an implicit solvation model. We chose to model the entire molecules, especially since none were too large for the available computer hardware. He et al. used the more expensive Møller-Plesset (MP2) method, yet we found that reliable results can be obtained using cheaper DFT methods and, in fact, MP2 is inferior to many DFT functionals in predicting vibrational frequencies, which are the basis of the Bigeleisen-Mayer equation (Eq. 4) (Iron & Gropp, 2019). In addition, in some cases, long-range interactions, such as hydrogen bonds, may affect the vibrational frequency of the primary site, and these effects might be overlooked if truncations are applied without the appropriate considerations. A careful truncation of molecules can be effective, but it does introduce a new potential source of error.

3 RESULTS

We calculated the RPFRs for position-specific single ^{13}C or D substitutions and double ^{13}C–D substitutions of the molecules that participate in anaerobic methane metabolisms at the M06-L/def2-TZVP level of theory (Full details in Section 2.2). The results of these calculations are presented in Tables 2–4, Table S.1 and Table S.2. The $^{13}\beta$ and $^{2}\beta$ values at 0-100 °C are presented in Fig. 2. In general, $^{13}\beta$, $^{2}\beta$ and ^{13,2}RPFR values at 25 °C covary with the carbon oxidation state, with the exception of the $^{13}\beta$ values for the methyl and carbonyl groups in CH_3-COSCoA, the $^{13}\beta$ for the methyl group in CH_3-COOH, and the $^{2}\beta$ and ^{13,2}RPFR values for CHO-MFR, CHO-H_4MPT and CH≡H_4MPT$^+$ (Tables 2–4).

We calculated the EFFs (α^{eq}) for the enzymatic reactions in the hydrogenotrophic, acetoclastic and methylotrophic methanogenesis pathways. The full results at 25 °C, 50 °C and 75 °C are provided in Table 5 and Figs. 3-4. For each reaction, we report α-values based on β and RPFR values through the relation ${}^{r}\alpha^{eq}_{A-B} = \beta_A/\beta_B$, where we arbitrarily chose compounds A to be upstream of compounds B in the methanogenesis pathway. For convenience, we follow the convention of reporting EFFs as a natural logarithm of ${}^{r}\alpha^{eq}_{A-B}$ in permil (‰) units (1000lnα). The fractionations of reactions involving H_2O are reported relative to $H_2O_{(l)}$. As calculation of the RPFR for liquid H_2O is notoriously challenging, we chose to apply the approach used by Wang et al., (2009a) and calculate $^{2}\beta$ of $H_2O_{(g)}$ and use the ${}^{2}\alpha^{eq}_{H_2O_{(l)}-H_2O_{(g)}}$ reported for the range 0-374 °C (Horita & Wesolowski, 1994), where ${}^{2}\beta_{H_2O_{(l)}} = {}^{2}\beta_{H_2O_{(g)}} \times {}^{2}\alpha^{eq}_{H_2O_{(l)}-H_2O_{(g)}}$.

Notably, the carbon isotope fractionations of the reactions in the hydrogenotrophic pathway, which add up to the net CO_2–CH_4 carbon isotope fractionation, distribute almost evenly among four steps in the pathway, three of which are carbon reduction reactions. The CO_2–CHO-MFR, CH≡H_4MPT$^+$–CH_2=H_4MPT, CH_2=H_4MPT–CH_3-H_4MPT and CH_3-H_4MPT–CH_3-SCoM carbon isotope fractionations are all between ∼14‰ and ∼18‰, whereas the other reactions yield smaller positive or small negative fractionations (Table 5). For hydrogen, primary isotope effects, in which a C–H bond is broken or made, produce larger positive or negative hydrogen isotope fractionations than secondary isotope effects, in which C–H bonds remain intact, besides the reaction between F_420H_2 and CH_3-H_4MPT which has a small primary EFF compared to its secondary EFFs (Fig. 4).

Using the RPFR values of the singly- and doubly-substituted isotopologues, we calculated the equilibrium deviation of clumped isotopologues from a stochastic distribution at equilibrium (Δ_i^{eq}) of each intermediate metabolite in the methanogenic pathways, as well as the clumped isotope fractionations of reactions that involve doubly-substituted isotopologues ($^{13,2}\alpha$). In general, the Δ_i values increase with decreasing oxidation state, from $\Delta^{eq}_{^{13}\text{CDO-H}_4\text{MPT}} = 4.211‰$ to $\Delta^{eq}_{^{13}\text{CH}_3\text{D}} = 5.738‰$ at 25 °C, and they depend inversely on temperature (Fig. S.1). The $^{13,2}\alpha^{eq}$ values are similar in magnitude to the corresponding product of $^{13}\alpha^{eq}$ and $^{2}\alpha^{eq}$, but not equal, as demonstrated by the

positive Δ_i^{eq} values that we calculated. As suggested by Wang et al. (2015), the clumped isotope fractionation factor can be expressed as ${}^{13,2}\alpha^{eq} = {}^{13}\alpha^{eq} \times {}^{2}\alpha^{eq} \times {}^{13,2}\gamma$, where the unitless ${}^{13,2}\gamma$ factor is a measure of the deviation of the fractionation from the expected stochastic distribution (Fig. 5). For secondary isotope effects, where the ^{13}C–D bond remains intact, ${}^{13,2}\gamma$ is very close to unity with a mean of –0.17‰ at 25 °C due to the similar magnitude of the Δ_i^{eq} values. For primary isotope effects, where a ^{13}C–D bond is formed or broken, ${}^{13,2}\gamma$ is larger and can be directly related to the Δ_i^{eq} of the reaction product through $\Delta_i^{eq} = \left(1/{}^{13,2}\gamma\right) - 1$.

4 DISCUSSION

4.1 Beta values

The principles of equilibrium isotopic fractionation can explain the general trends observed in the calculated $^{13}\beta$, $^{2}\beta$ and ^{13,2}RPFR values, where at a given temperature these values decrease with the carbon oxidation state. The carbon oxidation state, ranging from +4 in CO_2 to –4 in CH_4, exerts first-order control over the carbon bonding environment, and specifically over the bond stiffness and strength. A higher oxidation state generally corresponds to stiffer bonds and consequently larger $^{13}\beta$, $^{2}\beta$ and ^{13,2}RPFR values at a given temperature. Similar correlations of β values and oxidation state have been observed for S (Eldridge et al., 2016), Fe (Fujii et al., 2014), and Se (Li & Liu, 2011) isotopic fractionations. A natural consequence of this correlation is that, in general, we may expect carbon reduction reactions to have carbon, hydrogen and clumped isotope EFFs larger than unity.

4.2 Uncertainties in calculated fractionation factors

The uncertainties in our predicted EFFs would best be estimated by comparison with experimentally determined isotopic fractionations. However, experimental evaluations of carbon, hydrogen and clumped isotopic fractionations among the intermediate, intracellular metabolites of all three methanogenic pathways have not yet been reported, with the exception of one investigation of the carbon and hydrogen isotopic fractionation among CH_3-SCoM, HS-CoB and CH_4. Moreover, in the methylotrophic and acetoclastic pathways, even measurements of equilibrium isotopic fractionations between the pathway end-members have not been reported. In the absence of experimental constraints on the isotopic fractionation factors, we follow the approach taken in previous studies for assessing the accuracy of DFT calculations of EFFs of large organic molecules. The 95% confidence interval (CI95) associated with the comparison of calculated and experimental hydrogen EFFs was found to be $\pm$5‰ to $\pm$10‰ for linear ketones (Wang et al., 2009a) and $\pm$10‰ to $\pm$30‰ for cyclic ketones (Wang et al., 2013), at the B3LYP/6-311G** level of theory. More recently, we extended the evaluation to isotopes of C, N and O (Iron & Gropp, 2019). The associated CI95 for C, N and O isotopes is $\pm$2.5‰. However, CI95 represents only the uncertainty in the parameters of the regression model, and the predictive power of our DFT calculations is more rigorously captured by the 95% prediction interval (PI95). The nonsimultaneous observation bounds of the PI95 are $\pm$30‰ for hydrogen isotopes and $\pm$8‰ for carbon isotopes. While the benchmark database on which these PI95 are based is limited in its coverage of different functional groups, we suggest that it is currently the most suitable alternative to experimental constraints when attempting to determine the actual magnitude of the uncertainty.

4.3 Comparisons with previous experimental and theoretical studies

To validate our calculated EFFs, we compare our results with previous experimental observations and theoretical predictions of EFFs.

4.3.1 Isotopic fractionation in the CO_2–CH_4–H_2O–H_2 system

The small, volatile end-members of the hydrogenotrophic methanogenesis pathway have been well characterized in both theoretical and experimental studies, and the efforts to better constrain the isotopic fractionations among them are ongoing. Four EFFs are of interest: (*i*) the CO_2–CH_4 carbon isotopic fractionation, (*ii*) the H_2O–H_2 hydrogen isotopic fractionation, (*iii*) the CH_4–H_2 hydrogen isotopic fractionation, and (*iv*) the CH_4–H_2O hydrogen isotopic fractionation. For hydrogen isotopes, we also present here the results using the HCTH/def2-TZVP level of theory. Overall, our predictions based on the M06-L/def2-TZVP and HCTH/def2-TZVP levels of theory yield good agreement with previous estimates of the fractionation factors, as discussed below.

Our results for case (*i*) agree with $1000\ln^{13}\alpha^{eq}_{CO_2-CH_4}$ values calculated using measured vibrational frequencies over a temperature range of 0-700 °C (Richet et al., 1977) and with experimental observations of $1000\ln^{13}\alpha^{eq}_{CO_2-CH_4}$ over a temperature range of 200-700 °C (Horita, 2001; Kueter et al., 2019) (Fig. 6a). To our knowledge, CO_2–CH_4 carbon isotopic fractionations have not been experimentally measured below 200 °C, but the agreement of our theoretical predictions with the available, high-temperature experimental data provides confidence in our predictions at lower temperatures.

For case (*ii*), our $1000\ln^{2}\alpha^{eq}_{H_2O-H_2}$ values generally agree with previous experimental measurements at low and high temperatures (Cerrai et al., 1954; Rolston et al., 1976) (Fig. 6b). Rolston et al. (1976) measured fractionation between $H_2O_{(l)}$ and $H_{2(g)}$. Our H_2O–H_2 hydrogen isotopic fractionations using M06-L are comparable but slightly higher than other modeling studies based on spectroscopic data rather than DFT (Suess, 1949; Bardo & Wolfsberg, 1976). Our H_2O–H_2 hydrogen isotopic fractionation based on the HCTH functional produce a better fit to the observations, which is identical to the prediction of Bardo & Wolfsberg (1976).

In case (*iii*), our $1000\ln^{2}\alpha^{eq}_{CH_4-H_2}$ values calculated at the M06-L level of theory are larger by 40-45‰ than the values measured in the temperature range 200-500 °C (Horibe & Craig, 1995) (Fig. 6c), while the HCTH level of theory produces a better fit in this temperature range (only 10-30‰ larger than the experimental values). At this range of temperatures, there is disagreement between published theoretical estimates of the CH_4–H_2 equilibrium hydrogen isotopic fractionation (Bottinga, 1969; Richet et al., 1977). Our results agree with those of Richet et al. (1977) and are smaller by 0-30‰ than the fractionations calculated by Bottinga (1969). Of all published theoretical estimates of the CH_4–H_2 equilibrium hydrogen isotopic fractionation, our calculations at the HCTH level of theory are closest to the available high-temperature measurements. At temper-

atures lower than 100 °C, which are relevant for biological activity, there are no experimentally-determined CH_4–H_2 equilibrium hydrogen isotopic fractionations. At these temperatures there is an even larger discrepancy between all available theoretical predictions and a linear regression of ${}^2\alpha^{eq}_{CH_4-H_2}$ on 10^6/T, extrapolated from experimental results at 200-500 °C (Horibe & Craig, 1995). Reconciling these discrepancies is beyond the scope of the current study, requiring experiments to determine the CH_4–H_2 equilibrium hydrogen isotopic fractionations at temperatures lower than 200 °C.

For case (*iv*), there are no direct measurements of the CH_4–H_2O equilibrium hydrogen isotopic fractionation, $1000\ln{}^2\alpha^{eq}_{CH_4-H_2O_{(l)}}$, and a common practice is to combine available values of $1000\ln{}^2\alpha^{eq}_{CH_4-H_2}$ and $1000\ln{}^2\alpha^{eq}_{H_2-H_2O_{(l)}}$. There is a striking disagreement among the different combinations of $1000\ln{}^2\alpha^{eq}_{CH_4-H_2}$ and $1000\ln{}^2\alpha^{eq}_{H_2-H_2O_{(l)}}$ values, with $1000\ln{}^2\alpha^{eq}_{CH_4-H_2O_{(l)}}$ ranging from –110 to –300‰ at 0 °C and from –85 to –210‰ at 60 °C (Fig. 7a). Most of this spread stems from the uncertainty in $1000\ln{}^2\alpha^{eq}_{CH_4-H_2}$ values at low temperatures. To date, most interpretations of environmental $1000\ln{}^2\alpha^{eq}_{CH_4-H_2O_{(l)}}$ values rely on the extrapolation of the 200-500 °C experimental results (Horibe & Craig, 1995) to environmentally-relevant temperatures (e.g., Proskurowski et al., 2006; Wang et al., 2017). As noted above, this extrapolation does not agree with any method of theoretical calculation. We collected from the literature 165 environmental samples of biological origin from marine sediments and gas reservoirs (Table S.3) and compared their measured CH_4–$H_2O_{(l)}$ hydrogen isotopic fractionation to the calculated temperature-dependent $1000\ln{}^2\alpha^{eq}_{CH_4-H_2O_{(l)}}$ (Fig. 7a–b). We also compiled 183 values of measured CO_2–CH_4 carbon isotopic fractionations from the same locations and their deviation from the expected temperature-dependent $1000\ln{}^{13}\alpha^{eq}_{CO_2-CH_4}$ (Fig. 7c). We found that the distribution of the deviations of the CO_2–CH_4 apparent carbon isotopic fractionation from isotopic equilibrium has a distinct peak at zero, which we interpret as evidence of carbon isotope equilibration in the CO_2–CH_4 system. This may suggest that the hydrogen isotopes in the CH_4–H_2O system are also at (or close to) isotopic equilibrium. If this is the case, the distribution of compiled apparent hydrogen isotopic fractionations may inform the choice of DFT theory and constrain the error on our calculated hydrogen isotopic fractionation factors. The distribution of the deviation of the CH_4–$H_2O_{(l)}$ apparent hydrogen isotopic fractionation from isotopic equilibrium calculated with the M06-L functional has a distinct peak at zero, whereas with HCTH the distribution peaks at ∼20‰, suggesting that the M06-L functional provides a more accurate prediction in this case.

4.3.2 Isotopic fractionation between large organic molecules in the methanogenesis pathway

To our knowledge, the equilibrium hydrogen isotopic fractionation between CH_3-SCoM and CH_4 ($\ln{}^2\alpha^{eq}_{CH_3\text{-SCoM}-CH_4}$) is the only experimentally determined fractionation between intracellular intermediate metabolites in the methanogenesis pathway. Scheller et al. (2013) investigated the kinetic isotopic fractionation in the Mcr-catalyzed reaction, the final step in methanogenesis. EFFs

can be calculated from the kinetic fractionation factors (KFFs) of the reverse and forward reactions: ${}^{r}\alpha^{\mathrm{eq}}_{\mathrm{A-B}} = {}^{r}\alpha^{\mathrm{kin}}_{\mathrm{B\rightarrow A}}/{}^{r}\alpha^{\mathrm{kin}}_{\mathrm{A\rightarrow B}}$, where ${}^{r}\alpha^{\mathrm{kin}}_{\mathrm{B\rightarrow A}}$ and ${}^{r}\alpha^{\mathrm{kin}}_{\mathrm{A\rightarrow B}}$ are the reverse and forward KFFs, respectively. While Scheller et al. (2013) did not report $1000\ln{}^{2}\alpha^{\mathrm{eq}}_{\mathrm{CH_3\text{-}SCoM-CH_4}}$, we calculated a value of 17±42‰ at 60 °C, based on their measured ${}^{2}\alpha^{\mathrm{kin}}_{\mathrm{CH_3\text{-}SCoM\rightarrow CH_4}}$ (0.840±0.01) and ${}^{2}\alpha^{\mathrm{kin}}_{\mathrm{CH_4\rightarrow CH_3\text{-}SCoM}}$ (0.855±0.05) taking into account error propagation. Our calculated value of 40.4‰ at this temperature is within error of the experimental value.

4.3.3 $\Delta^{\mathrm{eq}}_{^{13}\mathrm{CH_3D}}$

For methane, our predictions of $\Delta^{\mathrm{eq}}_{^{13}\mathrm{CH_3D}}$ in thermodynamic equilibrium agree well with previous theoretical and experimental estimates (Webb & Miller, 2014; Liu & Liu, 2016; Eldridge et al., 2019). There are currently no available measurements of the intermediates in the methanogenesis pathway to which we can compare our results.

4.4 Implications of predicted EFFs for methanogenesis and methanotrophy

Methanogenesis is characterized by large and variable CO_2–CH_4 carbon isotopic fractionations (tens of permil) and CH_4–H_2O hydrogen isotopic fractionations (hundreds of permil). Variation within these ranges has been hypothesized to be controlled by the degree of reversibility of the enzymatically-catalyzed reactions (Valentine et al., 2004; Wang et al., 2015; Stolper et al., 2015). The net isotopic fractionation of any individual biochemical reaction varies between thermodynamic and kinetic end-members. The thermodynamic end-member is the product of a fully reversible reaction, and it gives rise to a substrate-product isotopic fractionation equal to the EFF between these compounds. The kinetic end-member is well-defined for a single reaction as the isotopic fractionation when that reaction is unidirectional, and it is equal to the ratio of the isotope-specific rate constants of the reaction. The kinetic end-member depends on the reaction mechanism, which depends on the structure of the enzyme catalyzing the reaction, and on the exact substrates participating in the reaction. Thus, the kinetic end-member may vary for different microbial strains and physiological conditions.

As a reaction departs from equilibrium, for example in response to an increase in substrate concentration, its isotopic fractionation will transition smoothly from equilibrium to the kinetic fractionation (DePaolo, 2011; Wing & Halevy, 2014). For the reaction $r \rightleftarrows p$, the net isotopic fractionation from metabolite pools r to p at a steady state ($\alpha^{\mathrm{net}}_{r-p}$) can be calculated from the EFF ($\alpha^{\mathrm{eq}}_{r-p}$), the forward KFF ($\alpha^{\mathrm{kin}}_{r\rightarrow p}$) and the ratio of the backward and forward mass fluxes of the reaction ($f_{p,r}$):

$$\alpha^{\mathrm{net}}_{r-p} = \left(\alpha^{\mathrm{eq}}_{r-p} - \alpha^{\mathrm{kin}}_{r\rightarrow p}\right) f_{p,r} + \alpha^{\mathrm{kin}}_{r\rightarrow p}. \tag{8}$$

The thermodynamic end-member is expressed when the reaction is fully reversible ($f_{p,r}$ = 1) and Eq. 8 reduces to $\alpha^{\mathrm{net}}_{r-p} = \alpha^{\mathrm{eq}}_{r-p}$. The kinetic end-member is expressed when the reaction is uni-

directional ($f_{p,r}$ = 0), and Eq. 8 reduces to $\alpha^{\text{net}}_{r-p} = \alpha^{\text{kin}}_{r\to p}$. In a linear reaction network with the metabolite pools s, r and p such as $s \rightleftarrows r \rightleftarrows p$, different steps have fractionations that differentially depart from their individual thermodynamic equilibrium fractionation end-members to give a range of disequilibrium fractionations of the total reaction network (Wing & Halevy, 2014). The net isotopic fractionation between s and p at a steady state can be calculated from the recursive expression:

$$\alpha^{\text{net}}_{s-p} = \left(\alpha^{net}_{r-p} \times \alpha^{eq}_{s-r} - \alpha^{\text{kin}}_{s\to r}\right) f_{r,s} + \alpha^{\text{kin}}_{s\to r} \tag{9}$$

(See Appendix A and Wing & Halevy (2014) for more detiles). In this case, the thermodynamic end-member is expressed when both reactions are fully reversible ($f_{r,s} = f_{p,r}$ = 1) and Eq. 9 reduces to $\alpha^{\text{net}}_{s-p} = \alpha^{\text{eq}}_{r-p} \times \alpha^{\text{eq}}_{s-r}$. The kinetic end-member is expressed when the most upstream reaction is unidirectional ($f_{r,s}$ = 0), and Eq. 9 reduces to $\alpha^{\text{net}}_{s-p} = \alpha^{\text{kin}}_{s\to r}$. A range of disequilibrium net isotopic fractionations between these values is expressed upon progressive departure from equilibrium (e.g., with increasingly negative ΔG_r), and the transition may not be monotonic due to the dependence on the reversibilities and KFFs of individual reactions. This approach is only applicable to linear metabolic networks, and we use it here to explore the possible effect of the ΔG_r (and rate) of hydrogenotrophic and acetoclastic methanogenesis and anaerobic methanotrophy on the carbon isotopic fractionation (Sections 4.4.1, 4.4.4 and 4.4.5).

In some metabolic networks, the isotope exchange reaction involves three compounds rather than two, such as for hydrogen atoms in the hydrogenotrophic pathway. For example, in the reaction $a\mathrm{Y}_n + b\mathrm{Y}_m \rightleftarrows c\mathrm{Y}_{n+m}$, where a, b and c are arbitrary organic residues, Y is the atom of interest and n and m are the stoichiometric coefficients of Y. For brevity, we will denote this reaction as $r_1 + r_2 \rightleftarrows p$, where r_1 is $a\mathrm{Y}_n$, r_2 is $b\mathrm{Y}_m$ and p is $c\mathrm{Y}_{n+m}$. The change of the isotopic composition of compound p with time can be expressed as:

$$\frac{d}{dt}\cdot R_p = \frac{1}{[p]}\Big[\phi_{rp}\left(n\cdot\alpha^{\text{kin}}_{r_1\to p}R_{r_1} + m\cdot\alpha^{\text{kin}}_{r_2\to p}R_{r_2}\right) - \phi_{pr}\cdot R_p\left(n\cdot\alpha^{\text{kin}}_{p\to r_1} + m\cdot\alpha^{\text{kin}}_{p\to r_2}\right) - R_p(m+n)\left(\phi_{rp}-\phi_{pr}\right)\Big], \tag{10}$$

where ϕ_{rp} and ϕ_{pr} are the net forward and reverse mass fluxes, respectively, and R_{r_1}, R_{r_2} and R_p are the ratios of the rare and abundant isotopes in pools r_1, r_2 and p, respectively. In the specific case of a chemical and isotopic steady state, the isotopic composition of p is constant, and $\frac{d}{dt}\left([p]\cdot R_p\right) = 0$. Rearranging the equation yields an analytical solution for R_p at a steady state:

$$R_p = \frac{\phi_{rp}\left(n\cdot\alpha^{\text{kin}}_{r_1\to p}R_{r_1} + m\cdot\alpha^{\text{kin}}_{r_2\to p}R_{r_2}\right)}{\phi_{pr}\left(n\cdot\alpha^{\text{kin}}_{p\to r_1} + m\cdot\alpha^{\text{kin}}_{p\to r_2}\right) + (m+n)\left(\phi_{rp}-\phi_{pr}\right)} \tag{11}$$

(see full derivation of Eqs. 10 and 11 in Appendix B.1). In a metabolic network with multiple sources of an atom of interest, extending the expression in Eq. 11 is impractical, unless we impose constraints over the values of the mass fluxes and isotope effects (e.g., Cao et al., 2019). To

avoid prior assumptions, the net isotopic fractionations in such a system can be determined numerically by solving an isotopic mass balance such as in Eq. 10 for every metabolite as a set of ordinary differential equations. The numerical solutions do not provide the same intuition as analytical expressions, and in some cases the systems can be simplified to produce an approximate analytical solution. Next, we will discuss one such simplified analytical solution for the hydrogen isotopic fractionation between CH_4 and H_2O in the hydrogenotrophic pathway (Section 4.4.2) and a numerical solution for carbon isotopic fractionation in the methylotrophic pathway (Section 4.4.3). In both cases we discuss isotopic fractionations observed in laboratory cultures or environmental samples. These apparent isotopic fractionations between compounds A and B is defined by ${}^{r}\alpha_{\mathrm{A-B}} \equiv {}^{r}R_{\mathrm{A}}/{}^{r}R_{\mathrm{B}}$ and presented using the $1000\ln{}^{r}\alpha_{\mathrm{A-B}}$ notation. These isotopic fractionations represent combinations of the equilibrium and kinetic isotopic fractionations (Section 4.4) and should not be confused with the EFFs ($1000\ln{}^{r}\alpha^{\mathrm{eq}}_{\mathrm{A-B}}$) or KFFs ($1000\ln{}^{r}\alpha^{\mathrm{kin}}_{\mathrm{A\rightarrow B}}$).

4.4.1 Carbon isotopes in the hydrogenotrophic pathway

Fractionation of carbon isotopes in the hydrogenotrophic methanogenesis pathway ($1000\ln{}^{13}\alpha_{\mathrm{CO_2-CH_4}}$) ranges from ∼10‰ to ∼90‰ in laboratory cultures, and correlates with the net ΔG_r and the cell-specific rate of methanogenesis (Valentine et al., 2004; Penning et al., 2005; Takai et al., 2008; Okumura et al., 2016; Topçuoğlu et al., 2019). Cultures grown at small negative ΔG_r (e.g., low concentrations of H_2) often show $1000\ln{}^{13}\alpha_{\mathrm{CO_2-CH_4}}$ values larger than the equilibrium carbon isotopic fractionation (the temperature-dependent EFF). For example, batch cocultures of methanogens and syntrophic partners grown on propionate at 37 °C have apparent $1000\ln{}^{13}\alpha_{\mathrm{CO_2-CH_4}}$ values of 64‰-89‰ with a mean of 78‰ (Penning et al., 2005), larger than the calculated temperature-dependent EFF of 64.8‰ at the same temperature. Batch cocultures grown on formate at 82 °C have apparent $1000\ln{}^{13}\alpha_{\mathrm{CO_2-CH_4}}$ values of 73‰-85‰, again larger than the temperature-dependent calculated EFF of 53.45‰ (Topçuoğlu et al., 2019). Larger-than-equilibrium carbon isotopic fractionations have also been observed in pure cultures grown in chemostats although with smaller deviations from the EFF, probably because the departure from equilibrium was large enough (i.e., ΔG_r was negative enough) that the combined reversibilities and KFFs resulted in smaller net isotopic fractionations (Valentine et al., 2004; Topçuoğlu et al., 2019). Larger-than-equilibrium carbon isotopic fractionations have also been observed in incubation experiments with deep aquifer groundwater (Hattori et al., 2012). We compiled the apparent $1000\ln{}^{13}\alpha_{\mathrm{CO_2-CH_4}}$ values available in the literature for pure culture, coculture and enrichment experiments. Comparing these measurements with the calculated temperature-dependent EFFs we found a bimodal distribution with peaks at +10‰ and –20‰ (Fig. S.2). Most of the values larger than the corresponding temperature-dependent EFF are from batch culture experiments. However, we only consider data that were not affected by Rayleigh distillation, that is, experiments where the isotopic composition of the substrates was similar to the initial isotopic composition throughout the experiment.

Previous models of microbial methanogenesis suggested various scenarios in which the reversibility of the metabolic pathway shapes the relationship between $1000\ln^{13}\alpha_{CO_2-CH_4}$ and ΔG_r or the cell-specific methanogenesis rate. In these models, the EFFs and f for the various steps in the reaction network were treated as free parameters. We used our calculated EFFs at 25 °C and the mathematical framework for linear metabolic networks outlined in Section 4.4 to explore some of the previously suggested scenarios:

(*i*) Gradual and uniform departure from equilibrium of all steps in the pathway (Wang et al., 2015).

(*ii*) Isotopic equilibrium between CO_2 and CH_3-H_4MPT or CH_3-SCoM, and variable reversibility of the Mtr- or Mcr-catalyzed reactions (Alperin & Hoehler, 2009; Stolper et al., 2015).

(*iii*) Differential reversibility of the different reactions in the pathway (Cao et al., 2019).

For each scenario, we used some combination of f values in the recursive term in Eq. 9 to estimate $1000\ln^{13}\alpha_{CO_2-CH_4}$ (Table 7). We assigned $1000\ln^{13}\alpha^{kin}$ of 20‰ for all the reactions in the pathway, except for $1000\ln^{13}\alpha^{kin}_{CH_3\text{-SCoM}\rightarrow CH_4}$, which has been experimentally measured to be ∼40‰ (Scheller et al., 2013). Details of the calculations are in Appendix A).

In scenario (*i*) of uniform departure from reversibility, the minimal, kinetic end-member $1000\ln^{13}\alpha_{CO_2-CH_4}$ value (i.e., when $f = 0$) is 20‰, consistent with fractionations measured at large negative ΔG_r. In this case, only the KFF of the most upstream, Fmd-catalyzed reaction ($\ln^{13}\alpha^{kin}_{CO_2\rightarrow CHO\text{-}MFR}$) is expressed, and the net fractionations of the other reactions in the network (in this case, all $^{13}\alpha^{kin}$ values as $f = 0$) are not expressed (Eq. 9). The maximal $1000\ln^{13}\alpha_{CO_2-CH_4}$ depends on the $^{13}\alpha^{kin}$ values assigned to the different reactions. For $^{13}\alpha^{kin}$ values smaller than 60‰, the maximal $1000\ln^{13}\alpha_{CO_2-CH_4}$ is the thermodynamic equilibrium carbon isotopic fractionation of 69‰. Larger-than-equilibrium $1000\ln^{13}\alpha_{CO_2-CH_4}$ values require $^{13}\alpha^{kin}$ values larger than 60‰. For example, a $1000\ln^{13}\alpha_{CO_2-CH_4}$ value of 75‰ at 25 °C would require $^{13}\alpha^{kin}$ values of ∼80‰ for the reactions catalyzed by Mtd, Mer and Mtr. Though we cannot rule them out, to the best of our knowledge carbon isotope KFFs of such magnitude have not been measured. Within the limits of observed carbon isotope KFFs, the assumption of a uniform departure from equilibrium places a hard limit on the maximum value of $1000\ln^{13}\alpha_{CO_2-CH_4}$, which is smaller than the observed net carbon isotopic fractionation.

In scenario (*ii*), the reactions from CO_2 to CH_3-SCoM are fully reversible (i.e., $f = 1$), and only the most downstream, Mcr-catalyzed reaction departs from reversibility. When implemented in the framework described above, the range of possible $1000\ln^{13}\alpha_{CO_2-CH_4}$ is 69-106‰. The maximal $1000\ln^{13}\alpha_{CO_2-CH_4}$ value is due to substitution of the small CH_3-SCoM–CH_4 EFF (we calculated 1.6‰ at 25 °C) by the much larger KFF of the Mcr-catalyzed step (40‰; Scheller et al., 2013). In this scenario, $1000\ln^{13}\alpha_{CO_2-CH_4}$ cannot be smaller than 69‰, which is inconsistent with the

large number of $1000\ln^{13}\alpha_{CO_2-CH_4}$ measurements that are smaller than this value, and suggesting that the departure from equilibrium of the last steps in the pathway cannot be the sole process responsible for the observed range of CO_2–CH_4 carbon isotopic fractionation.

In scenario (*iii*), Cao et al. (2019) explored combinations of differential reversibility in methanogenesis, focusing on clumped isotopologues. They suggested binary f values (either 0 or 1) for the reactions catalyzed by Fmd, Mtd, Mer and Mcr. Using our calculated EFFs, we find that the binary scenarios yield $1000\ln^{13}\alpha_{CO_2-CH_4}$ covering the range of observed values (20-106‰). The largest $1000\ln^{13}\alpha_{CO_2-CH_4}$ value is obtained, as in scenario (*ii*), when f = 0 for the Mcr-catalyzed reaction and f = 1 for all other reactions in the pathway. In this case, a combination of the KFF of the Mcr-catalyzed reaction (40‰) with the equilibrium CO_2–CH_3-SCoM carbon isotopic fractionation (∼69‰) leads to the net $1000\ln^{13}\alpha_{CO_2-CH_4}$ of 109‰. The smallest $1000\ln^{13}\alpha_{CO_2-CH_4}$ is obtained, as in scenario (*i*), when f = 0 for the Fmd-catalyzed reaction, leading to expression of only the KFF of that reaction (prescribed to be 20‰).

We conclude that both scenarios (*i*) and (*iii*) are capable of covering the entire range of observed $1000\ln^{13}\alpha_{CO_2-CH_4}$. However, both scenarios invoke arbitrary combinations of the reversibility of the steps in the pathway, and scenario (*i*) also requires unrealistic carbon isotope KFFs. We note that in all models suggested to date, the reaction reversibilities were assigned rather than calculated, and it seems that a more detailed metabolic model is required to explain the nuances in the dependence of $1000\ln^{13}\alpha_{CO_2-CH_4}$ on ΔG_r.

4.4.2 Hydrogen isotopes in the hydrogenotrophic pathway

Fractionation of hydrogen isotopes during hydrogenotrophic methanogenesis in laboratory cultures ranges from ∼–100‰ to –600‰ and displays a weaker dependence on ΔG_r than the carbon isotopic fractionation (Valentine et al., 2004; Stolper et al., 2015; Okumura et al., 2016). Observed $1000\ln^{2}\alpha_{CH_4-H_2O}$ values deviate significantly from the expected CH_4–H_2O hydrogen isotope EFF (Fig. 6). For example, in two different experiments grown at 55°C and low H_2 concentrations (< tens of μM), one a coculture and the other a deep aquifer groundwater incubation, the $1000\ln^{2}\alpha_{CH_4-H_2O}$ values of –320±12‰ and –393±43‰, respectively, are significantly more negative than the temperature-dependent equilibrium fractionation of –175‰ at this temperature (Yoshioka et al., 2008; Hattori et al., 2012). Similar to carbon isotopes, such deviations of $1000\ln^{2}\alpha_{CH_4-H_2O}$ from the temperature-dependent hydrogen isotope EFF may arise from variations in the reversibility of the metabolic pathway, depending on the ΔG_r. In contrast to carbon isotopes, hydrogen isotope deviations from the EFF may also arise from mixing of hydrogen atom sources through direct incorporation of hydrogen atoms from H_2 in the Hmd-catalyzed reaction. There is ample evidence that this only occurs at high H_2 pressure or during exponential cell growth (e.g., Kawagucci et al., 2014; Okumura et al., 2016). Thus, it seems likely that the large, negative $1000\ln^{2}\alpha_{CH_4-H_2O}$ values observed in cultures grown at low H_2 concentrations are due to departure

from equilibrium and expression of KFFs, not incorporation of hydrogen from H_2.

Hydrogenotrophic methanogenesis involves the stepwise addition of four hydrogen atoms in four individual reactions (Fig. 1). Each of these additions is characterized by an individual net CH_4–H_2O hydrogen isotopic fractionation, which depends on the reaction reversibility and the equilibrium and kinetic end-member fractionations. The overall $1000\ln{}^2\alpha_{CH_4-H_2O}$ value depends on these individual fractionations in ways that may not be intuitive. In the extreme case that all hydrogen addition reactions are unidirectional (i.e., $f = 0$), for example at very large negative ΔG_r of the methanogenesis reaction, the overall $1000\ln{}^2\alpha_{CH_4-H_2O}$ value will be the average of the four KFFs associated with these reactions. As primary hydrogen isotope KFFs are generally large (e.g., ${}^{1000}{}^2\alpha^{kin}_{CH_3\text{-SCoM}\rightarrow CH_4}$ is ∼890‰ at 60 °C; Scheller et al., 2013), the expectation in this case is a substantially larger-than-equilibrium net $1000\ln{}^2\alpha_{CH_4-H_2O}$.

Unlike carbon isotopes, for which the reaction network is linear, there are four distinct steps in which exchange of hydrogen isotopes between methane and water may occur. The exchange does not occur directly with intracellular water, but through various intracellular metabolites with isotopic compositions that are related to that of the intracellular water. For example, in the Mcr-catalyzed reaction, one hydrogen atom is transferred from HS-CoB to CH_3-SCoM, yielding methane with a net CH_4–H_2O hydrogen isotopic fractionation that depends on the reversibility of this reaction. If the Mcr-catalyzed reaction fully departs from equilibrium ($f = 0$) to express its KFF, the total $1000\ln{}^2\alpha_{CH_4-H_2O}$ will deviate from the calculated EFF, even if the other three hydrogen addition reactions result only in equilibrium isotope effects. In this case (See Appendix B.1 for full derivation), the net CH_4–H_2O hydrogen isotope fractionation at a steady state between HS-CoB and methane is:

$$ {}^2\alpha^{net}_{CH_4-H_2O} = \frac{3}{4}\left({}^2\alpha^{kin}_{CH_3\text{-SCoM}\rightarrow CH_4}/{}^2\alpha^{eq}_{H_2O-CH_3\text{-SCoM}}\right) + \frac{1}{4}\left({}^2\alpha^{kin}_{HS\text{-CoB}\rightarrow CH_4}/{}^2\alpha^{eq}_{H_2O-HS\text{-CoB}}\right). \tag{12} $$

In other words, even if three of the four hydrogen atoms in CH_4 reflect equilibrium between H_2O and an intracellular CH_3-S-CoM intermediate, departure of the last hydrogen addition reaction from equilibrium will result in a disequilibrium net $1000\ln{}^2\alpha_{CH_4-H_2O}$. Using our calculated EFFs at 25 °C and literature KFFs for this reaction (${}^2\alpha^{kin}_{CH_3\text{-SCoM}\rightarrow CH_4} = 0.85$ and ${}^2\alpha^{kin}_{HSCoB\rightarrow CH_4} = 0.41$; Scheller et al., 2013) Eq. 12 yields a $1000\ln{}^2\alpha_{CH_4-H_2O}$ value of –507‰, compared to the calculated EFF of –195‰. The standard ΔG_r (ΔG^0_r) of Mcr is ∼–30 kJ mol^{-1}, and it has been suggested that during methanogenesis the last hydrogen addition reaction is effectively irreversible (Thauer, 2011). Eq. 12 demonstrates how the KFFs that are associated with Mcr are sufficient to drive deviations of the net CH_4–H_2O hydrogen isotopic fractionation from equilibrium by more than 300‰.

On the other hand, if the Hdr- and Mcr-catalyzed reactions are at or close to equilibrium ($f \rightarrow 1$), disequilibrium upstream of the Mcr-catalyzed reaction does not impact the net CH_4–H_2O fractionation, which will reflect the equilibrium exchange of hydrogen isotopes between CH_4 and H_2O (via

HS-CoB):

$$^{2}\alpha^{\text{net}}_{\text{CH}_4-\text{H}_2\text{O}} = \left(^{2}\alpha^{\text{eq}}_{\text{HS-CoB}-\text{CH}_4} / ^{2}\alpha^{\text{eq}}_{\text{H}_2\text{O}-\text{HS-CoB}}\right). \quad (13)$$

Given the thermodynamic favorability of the Mcr-catalyzed hydrogen addition reaction, near-equilibrium of this reaction concurrent with disequilibrium of the upstream hydrogen additions is unlikely, and this hypothetical case serves only to illustrate the situation in which downstream equilibrium exchange of hydrogen isotopes with water (via HS-CoB) overprints upstream hydrogen isotopic fractionations. This is in contrast with linear reaction networks in which isotopic exchange only occurs among metabolites in the main reaction chain, such as carbon isotopes in methanogenesis or sulfur isotopes in dissimilatory sulfate reduction. In such linear networks, it is upstream kinetic control that mutes isotopic fractionation inherited from downstream reactions (Wing & Halevy, 2014), opposite to the hypothetical case discussed above.

4.4.3 Methylotrophic pathway

The methylotrophic pathway is underrepresented in the literature compared to the hydrogenotrophic pathway, and thus there is a smaller database with which to compare our results. Most of the data are from laboratory experiments, which are important as they are often used to assess the specific pathway of microbial methane production in the environment (e.g., Zhuang et al., 2018). However, the main controls on carbon and hydrogen isotopic fractionation in these pathways remain unclear, as do their dependencies on ΔG_r. Below, we discuss the implications of our predicted EFFs for the methylotrophic pathway, focusing on carbon isotopes.

Net carbon isotopic fractionation between methanol and methane $1000\ln{}^{13}\alpha_{\text{methanol}-\text{CH}_4}$ during methylotrophic methanogenesis in laboratory cultures spans a relatively narrow range of 67-83‰ (Krzycki et al., 1987; Londry et al., 2008; Penger et al., 2012, 2014), and methylotrophic enrichment cultures display carbon isotopic fractionations of up to 90‰ (Rosenfeld & Silverman, 1959). It is unclear whether these limited observations cover the entire range of physiologically relevant conditions, but it is clear that the range of $1000\ln{}^{13}\alpha_{\text{methanol}-\text{CH}_4}$ values is much larger than our predicted EFFs that are 19.1-20.9‰ at 25-40 °C. Methanol conversion to methane is a disproportionation pathway, where methanol molecules are either fully oxidized to CO_2 or reduced to methane (Fig. 1). Assuming that all methanol is used to produce chemical energy and not to generate biomass, a 3:1 ratio of reduction:oxidation ($R_{\text{r/o}}$) is expected to account for cycling of the electron carriers. However, $R_{\text{r/o}}$ may vary if the cells utilize some of the methanol to generate biomass, which requires reducing equivalents. The reducing equivalents in this case are reduced coenzyme F_{420} and ferredoxin, which are produced in the reverse methanogenesis pathway from CH_3-S-CoM to CO_2.

We explored the dependence of $1000\ln{}^{13}\alpha_{\text{methanol}-\text{CH}_4}$ and $1000\ln{}^{13}\alpha_{\text{methanol}-\text{CO}_2}$ on the reversibility of the pathway and on $R_{\text{r/o}}$, and to this end developed a simplified isotopic mass balance to find the isotopic fractionation in the methyltrophic pathway at steady state (see Appendix B.2).

We reduced the pathway to its three main branches: (1) from methanol to CH_3-S-CoM, (2) from CH_3-S-CoM to CH_4, and (3) from CH_3-S-CoM to CO_2. We assign KFFs in the range 30‰ to 50‰, assign a value to $R_{r/o}$, and use our calculated EFFs at 25 °C. We assume 75% reversibility between CH_3-SCoM and CO_2 (f_3 = 0.75), repeatedly (N = 10,000) pick random reversibility values for reactions 1 (f_1) and 2 (f_2) from a uniform distribution between 0 and 1, and calculate the possible range of $1000\ln^{13}\alpha_{\text{methanol}-\text{CH}_4}$ and $1000\ln^{13}\alpha_{\text{methanol}-\text{CO}_2}$ values (Table 7).

For $R_{r/o}$ = 3:1, $1000\ln^{13}\alpha_{\text{methanol}-\text{CH}_4}$ is 55-70‰, covering the lower range of the experimental observations. At $R_{\text{r/o}}$ = 1:1, the range of $1000\ln^{13}\alpha_{\text{methanol}-\text{CH}_4}$ shifts to 60-90‰ (Fig. 8, left), closer to the observed range and suggesting that the ratio of methanol reduction to oxidation may, in some cases, be appreciably lower than 3:1 due to a biosynthetic shunt. At the theoretical extreme case of $R_{\text{r/o}}$ = 20:1, there is almost no oxidation of methanol to CO_2, and the $1000\ln^{13}\alpha_{\text{methanol}-\text{CH}_4}$ range is 35-55‰. These small $1000\ln^{13}\alpha_{\text{methanol}-\text{CH}_4}$ values indicate that the oxidation to CO_2 is required to generate the observed range of carbon isotopic fractionation between methanol and CH_4. There are currently no known available measurements of methanol limitation conditions, and we have no indication whether at very low rates of methylotrophic methanogenesis $1000\ln^{13}\alpha_{\text{methanol}-\text{CH}_4}$ values approach the EFF.

In this study, we calculated an equilibrium methanol–CO_2 carbon isotopic fractionation ($1000\ln^{13}\alpha^{\text{eq}}_{\text{methanol}-\text{CO}_2}$ of –47.8‰ at 25 °C, while at $R_{\text{r/o}}$ = 3:1 our model predicts a range of net carbon isotopic fractionations between –25‰ and 0‰ (Fig. 8, right). At $R_{\text{r/o}}$ = 1:1, the range shifts to –20‰ to 20‰. The upper end of this range is similar to the ∼20‰ fractionations measured in a laboratory cultures (Penger et al., 2012). These values are complemented by the methanol-biomass and methanol-lipid carbon isotopic fractionations, which are also large and positive (>30‰; Londry et al., 2008) and which stem from the same metabolic branch. In our model, the large, positive $1000\ln^{13}\alpha_{\text{methanol}-\text{CO}_2}$ values required that the reversibility of the CH_3-SCoM to CO_2 branch is lower than 75%, because the calculated EFF is large and negative. At low reversibility of the methanol oxidation reaction, the net methanol–CO_2 fractionation shifts from the large, negative EFF to the large, positive KFF. Overall, this suggests a dominance of kinetic isotope effects in methylotrophic methanogenesis, at least under the conditions explored in laboratory culture experiments.

4.4.4 Acetoclastic pathway

The isotope effects in the acetoclastic pathway, similar to the methylotrophic pathway, are not well-studied. During acetoclastic methanogenesis, acetate dissociates to a methyl group (C_1), which is reduced to CH_3-H_4MPT and later released as CH_4, and to a carboxyl group (C_2), which is released as CO_2. The acetoclastic pathway has a smaller carbon isotopic fractionation between the substrate and CH_4 ($1000\ln^{13}\alpha_{\text{acetate}(\text{C}_1)-\text{CH}_4}$) than the hydrogenotrophic and methylotrophic pathways, with a range of 7-35‰ (Krzycki et al., 1987; Gelwicks et al., 1994; Penning et al.,

2006; Londry et al., 2008; Goevert & Conrad, 2009). Published measurements of the fractionation between the carboxyl group of acetate and CO_2 ($1000\ln^{13}\alpha_{\text{acetate}(C_2)-CO_2}$) are in the range of 35-47‰ in laboratory experiments and as low as 9‰ in a rice field soil incubation (Goevert & Conrad, 2009). We calculated the acetate–CH_4 and acetate–CO_2 carbon isotope EFFs of 16.3‰ and –13.3‰, respectively, at 25 °C. The equilibrium carbon isotopic fractionations between the C_1 atoms in acetate and those in acetyl-CoA and CH_3-H_4MPT are –0.4‰ and –3.3‰, respectively. The largest equilibrium carbon isotopic fractionation in this pathway is associated with the methyl group transfer between CH_3-H_4MPT and CH_3-S-CoM (17.9‰).

We explored the dependence of $1000\ln^{13}\alpha_{\text{acetate}(C_1)-CH_4}$ and $1000\ln^{13}\alpha_{\text{acetate}(C_2)-CO_2}$ on the reversibility of reactions in the pathway using the recursive expression in Eq. 9 for linear metabolic networks (details in Appendix A). A scenario of full reversibility (i.e., isotopic equilibrium) in the steps before the Mcr-catalyzed reaction and variable expression of ${}^{13}\alpha^{\text{kin}}_{CH_3\text{-SCoM}\rightarrow CH_4}$ yields a $1000\ln^{13}\alpha_{\text{acetate}(C_1)-CH_4}$ value between 16‰ and 53‰ at 25 °C depending on the reversibility of the Mcr-catalyzed reaction (Table 7). This calculated range covers most of the range observed in laboratory experiments, but it also dictates that $1000\ln^{13}\alpha_{\text{acetate}(C_2),CO_2}$ is equal to the acetate–CO_2 carbon isotope EFF (–13‰), much lower than the observed range. This suggests that the observed ranges of carbon isotopic fractionations between acetate and CO_2 or CH_4 are due to expression of kinetic isotope effects not only in the Mcr-catalyzed reaction but also in the first two reactions in the acetoclastic pathway (catalyzed by Ack/Pta and Cdh, Table 1).

4.4.5 Anaerobic methane oxidation

In reverse-methanogenesis AOM, the EFFs are the inverse of those in hydrogenotrophic methanogenesis, with the expected $1000\ln^{13}\alpha^{\text{eq}}_{CH_4-CO_2}$ in the range of –50‰ to –70‰, depending on temperature. To date, there are only a few measured $1000\ln^{13}\alpha_{CH_4-CO_2}$ and $1000\ln^{2}\alpha_{CH_4-H_2O}$ values of AOM in laboratory cultures, with ranges of 12-38‰ and 103-274‰, respectively (Holler et al., 2009). This enrichment of methane in ^{13}C and D contradicts the trends predicted by the EFFs for these reactions, suggesting that under the conditions of the available experimental results, the kinetic fractionation of carbon and hydrogen isotopes of steps in the pathway contributed to the observed net fractionations. There are limited observations at low sulfate availability (< 0.5 mM), in which methane is depleted in ^{13}C during AOM activity (Yoshinaga et al., 2014; Chuang et al., 2018). More specifically, Chuang et al. (2018) observed an apparent CH_4–CO_2 fractionation of –54.3‰ in the sulfate-methane transition zone (SMTZ), compared to the expected temperature-dependent EFF of –76.1‰ at 5 °C. In the case of AOM, a positive apparent $1000\ln^{13}\alpha_{CH_4-CO_2}$ is indicative of strong kinetic control over the system, whereas negative values, though not as negative as the EFFs, are indicative of joint expression of equilibrium and kinetic isotope effects.

To explore the possible control of the reversibility on $1000\ln^{13}\alpha_{CH_4-CO_2}$ during reverse-methanogenesis AOM, we used the recursive expression in Eq. 9 for linear metabolic networks (details in Appendix

A). We apply the approach of Cao et al. (2019) for methanogenesis, where we follow the carbon isotope reservoir effect of the seven reactions in the pathway (Table 7). We use the EFFs calculated in the present study at 25 °C, and calculate a $1000\ln^{13}\alpha^{\mathrm{kin}}_{\mathrm{CH_4\rightarrow CH_3\text{-}SCoM}}$ value of 38‰ based on the measured $1000\ln^{13}\alpha^{\mathrm{kin}}_{\mathrm{CH_3\text{-}SCoM\rightarrow CH_4}}$ value (40‰, Scheller et al., 2013) and our calculated $1000\ln^{13}\alpha^{\mathrm{eq}}_{\mathrm{CH_4-CH_3\text{-}SCoM}}$ (–2‰). For the rest of the pathway, we assume arbitrary but reasonable $1000\ln^{13}\alpha^{\mathrm{kin}}$ values of 5‰ or 40‰(Table 7).

We find that at steady state, a gradual expression of $1000\ln^{13}\alpha^{\mathrm{kin}}_{\mathrm{CH_4\rightarrow CH_3\text{-}SCoM}}$ (moving from f = 1 to 0) yields the largest $1000\ln^{13}\alpha_{\mathrm{CH_4-CO_2}}$ range of –69‰ to 37‰. The minimum value in this case is the calculated EFF, and the maximum value is the complete expression of $1000\ln^{13}\alpha^{\mathrm{kin}}_{\mathrm{CH_4\rightarrow CH_3\text{-}SCoM}}$ blocking any expression of isotope effects downstream of the reaction catalyzed by Mcr (Table 6). This covers the entire observed range of AOM $1000\ln^{13}\alpha_{\mathrm{CH_4-CO_2}}$ in lab cultures (12-38‰). However, it is not clear whether this reaction can actually be fully reversible due to its large-positive ΔG^0_r (+30 $\mathrm{kJ\,mol^{-1}}$) (Thauer, 2011). The same range can be obtained if the next downstream step between CH_3-SCoM and CH_3-H_4MPT imposes a reservoir effect and assuming a $1000\ln^{13}\alpha^{\mathrm{kin}}_{\mathrm{CH_3\text{-}SCoM\rightarrow CH_3\text{-}H_4MPT}}$ of 40‰, similar to the approach taken by Alperin & Hoehler (2009). As the isotope reservoir effect occurs further downstream in the AOM pathway, the range of net carbon isotopic fractionation becomes smaller, until finally the maximal $1000\ln^{13}\alpha_{\mathrm{CH_4-CO_2}}$ is between –50‰ and –15‰ depending on the magnitude of $^{13}\alpha^{\mathrm{kin}}_{\mathrm{CHO\text{-}MFR\rightarrow CO_2}}$.

5 CONCLUSIONS

This study provides a set of equilibrium carbon, hydrogen and clumped isotope fractionation factors associated with methanogenesis and anaerobic oxidation of methane, calculated by DFT at the M06-L/def2 TZVP level of theory and the SMD implicit solvation model. We compared our calculations to previous experimentally measured carbon and hydrogen isotope EFFs of the small, volatile end-members of these metabolic pathways (CO_2, CH_4, H_2O, H_2). Notably, we suggest that the CH_4–H_2O hydrogen isotope EFF at low (biologically-relevant) temperatures is probably more positive than the values obtained from extrapolation from high-temperature (>200 °C) experimental results. Experimental results with which to compare most of our calculated EFFs are absent, and we based our computational pipeline on a previous exploration of the optimal method of calculation of EFFs for large organic molecules.

We used our calculated EFFs to probe the isotopic fractionation among molecules in the most important metabolic pathways of anaerobic production and oxidation of methane—hydrogenotrophic, methylotrophic and acetoclastic methanogenesis, and anaerobic oxidation of methane. In these pathways, the net isotopic fractionation between the reactants and products are determined by a combination of EFFs and KFFs, and the degree of expression of each depends on the metabolic state of the organisms. In extremely energy-limited environments, the extracellular reactants and products may be in isotopic equilibrium. In this case, the intracellular reactions will also be at or close to equilibrium, each expressing its respective EFF. If more energy is available, departure from equilibrium of some (but not necessarily all) of the intracellular reactions in the pathway results in net fractionations that reflect a combination of their respective EFF and KFF, the contribution of which depends on the degree of departure of the reactions from equilibrium.

In the hydrogenotrophic methanogenesis pathway, we suggest that the large range of CO_2–CH_4 carbon isotope fractionations is a product of differential departure from reversibility along the metabolic pathway, rather than a uniform departure of all reactions or a departure of only one of the reactions from equilibrium. In the methylotrophic pathway, the calculated CH_3-OH–CH_4 carbon isotope fractionation is smaller than the apparent fractionations observed in environmental and laboratory culture samples by at least 50‰. Using a numerical solution to a simplified model of the methylotrophic pathway, we suggest that the large observed carbon isotope fractionations are due to utilization of some of the electrons from methanol to fix biomass rather than to produce methane, resulting in a higher proportion of methanol oxidation to CO_2 than reaction stoichiometry would dictate in the absence of biomass fixation.

The simplified examples discussed in this work provide a glimpse of the insights into complex biological systems, made available by accurate determination of equilibrium isotope fractionation factors. In the future, the comprehensive set of EFFs calculated here can be used in investigations of biologically-induced isotope effects in methanogenesis and AOM, to expand our understanding

693 of the interaction between microorganisms and their environment, and the way in which these
694 interactions are recorded in the stable isotope composition of natural materials.

6 Acknowledgments

We acknowledge support from the European Research Council Starting Grant No. 337183. J. G. acknowledges support from the Weizmann Institute Sustainability and Energy Research Initiative.

Table 1: **Enzymes that are included in this report and the reactions they catalyze.** The hydrogen and carbon atoms of interest are shown in bold. Note that we include only the reactions that participate in carbon and hydrogen isotope exchange during methanogenesis and AOM.

#	Enzyme	Reactant		Product
1	Fmd*	$\mathbf{C}O_2 + Fd_{red} + MFR + 2\,H^+$	$\rightleftarrows$	$\mathbf{CH}O\text{-}MFR + Fd_{ox} + H_2O$
2	Ftr	$\mathbf{CH}O\text{-}MFR + H_4MPT$	$\rightleftarrows$	$\mathbf{CH}O\text{-}H_4MPT + MFR$
3	Mch	$\mathbf{CH}O\text{-}H_4MPT + H^+$	$\rightleftarrows$	$\mathbf{CH}\equiv H_4MPT^+ + H_2O$
4	Mtd	$\mathbf{CH}\equiv H_4MPT^+ + F_{420}\mathbf{H}_2$	$\rightleftarrows$	$\mathbf{CH}_2 = H_4MPT + F_{420} + H^+$
5	Hmd	$\mathbf{CH}\equiv H_4MPT^+ + \mathbf{H}_2$	$\rightleftarrows$	$\mathbf{CH}_2 = H_4MPT$
6	Mer	$\mathbf{CH}_2 = H_4MPT + F_{420}\mathbf{H}_2$	$\rightleftarrows$	$\mathbf{CH}_3\text{-}H_4MPT + F_{420}$
7	Mtr	$\mathbf{CH}_3\text{-}H_4MPT + HS\text{-}CoM$	$\rightleftarrows$	$\mathbf{CH}_3\text{-}SCoM + H_4MPT$
8	Mcr	$\mathbf{CH}_3\text{-}SCoM + \mathbf{H}S\text{-}CoB$	$\rightleftarrows$	$\mathbf{CH}_4 + CoM\text{-}S\text{-}S\text{-}CoB$
9	Frh*	$H_2 + F_{420}$	$\rightleftarrows$	$F_{420}\mathbf{H}_2$
10	Hdr*	$H_2 + CoM\text{-}S\text{-}S\text{-}CoB + Fd_{ox}$	$\rightleftarrows$	$\mathbf{H}S\text{-}CoB + HS\text{-}CoM + Fd_{red} + 2\,H^+$
11	Mta	$\mathbf{CH}_3OH + HS\text{-}CoM$	$\rightleftarrows$	$\mathbf{CH}_3\text{-}SCoM + H_2O$
12	Ack/Pta	$\mathbf{CH}_3\text{-}\mathbf{C}OO^- + ATP + CoA\text{-}SH$	$\rightleftarrows$	$\mathbf{CH}_3\text{-}\mathbf{C}OSCoA + ADP + HPO_4^{2-}$
13	Cdh	$\mathbf{CH}_3\text{-}\mathbf{C}OSCoA + H_4MPT + Fd_{ox}$	$\rightleftarrows$	$\mathbf{CH}_3\text{-}H_4MPT + \mathbf{C}O_2 + CoA\text{-}SH + Fd_{red}$

* In these reactions, the source of the hydrogen atom is a proton from H_2O, while H_2 is the electron donor of the reaction.

Abbreviations: Fmd - formyl-methanofuran dehydrogenase; Ftr - formyl transferase; Mch - methylene-H_4MPT cyclohydrolase; Mtd - F_{420}-dependent methylene-H_4MPT dehydrogenase; Hmd - H_2-forming methylene dehydrogenase; Mer - methylene-H_4MPT reductase; Mtr - methyl transferase; Mcr - methyl-CoM reductase; Frh - F_{420}-reducing hydrogenase; Hdr - heterodisulfide reductase; Mta - methanol:coenzyme M methyltransferase; Ack - acetate kinase; Pta - phospho-transacetylase; Cdh - CO-dehydrogenase/acetyl-CoA synthase; MFR - methanofuran; H_4MPT - tetrahydromethanopterin; F_{420} - oxidized coenzyme F_{420}; $F_{420}H_2$ - reduced coenzyme F_{420}; Fd - ferredoxin; HS-CoM - Coenzyme M; HS-CoB - Coenzyme B; CoM-S-S-CoB - heterodisulfide; CoA-SH - coenzyme A.

Table 2: **Coefficients for the fourth-order polynomial fits to $^2\beta$ values.** Computed at the M06-L/def2-TZVP level of theory, between 273.15 and 973.15 K (0-700 °C). The fit to all values is of the form $A \times 10^{12}/T^4 + B \times 10^9/T^3 + C \times 10^6/T^2 + D \times 10^3/T + E$. For compounds with two or more inequivalent hydrogen atoms, the position-specific isotope substitutions are marked in bold font. For compounds with steric centers, we present the relevant stereoisomers (pro-R or pro-S). For a full list of the RPFR values see Tables S.1 and S.2.

Compound	$A \times 10^{-3}$	$B \times 10^{-2}$	$C \times 10^{-2}$	$D \times 10^{-2}$	E	$^2\beta$ (25 °C)	C valence
C**H**O-MFR	188.700	–96.325	277.178	–250.764	2.011161	12.3172	+2
C**H**O-H_4MPT	174.276	–88.761	257.329	–230.847	1.925948	11.6957	+2
C**H**≡H_4MPT$^+$	202.677	–105.337	299.106	–270.939	2.089275	12.5539	+2
C$\mathbf{H}_2$=H_4MPT (pro-S)	238.998	–125.852	352.540	–333.294	2.342288	13.5825	0
C$\mathbf{H}_2$=H_4MPT (pro-R)	238.470	–125.587	351.946	–333.399	2.343234	13.5462	0
C$\mathbf{H}_3$-OH	190.193	–96.232	278.474	–250.075	2.003502	12.7025	–2
C$\mathbf{H}_3$-H_4MPT	187.409	–95.287	275.880	–247.777	1.994895	12.4834	–2
C$\mathbf{H}_3$-SCoM	170.244	–85.585	250.455	–219.282	1.878176	11.9506	–2
C$\mathbf{H}_3$-COOH	160.477	–80.086	236.737	–204.718	1.819687	11.6762	–3
C$\mathbf{H}_3$-COSCoA	164.030	–82.081	241.799	–209.912	1.840587	11.7892	–3
CH_4 (g)	134.531	–64.311	198.282	–161.302	1.643685	11.2990	–4
H_2O (g)	141.410	–66.149	207.302	–153.094	1.615920	12.7383	–
H_2 (g)	3.667	–0.730	12.521	28.365	0.904290	3.4528	–
$F_{420}\mathbf{H}_2$ (pro-S)	191.181	–98.557	282.447	–257.273	2.032984	12.1852	–
HS-CoB	35.269	–15.134	63.265	–30.315	1.112846	5.9661	–

Table 3: **Coefficients for the fourth-order polynomial fits to $^{13}\beta$ values.** Computed at the M06-L/def2-TZVP level of theory, between 273.15 and 973.15 K (0-700 °C). The fit to all values is of the form $A \times 10^{12}/T^4 + B \times 10^9/T^3 + C \times 10^6/T^2 + D \times 10^3/T + E$. For compounds with two or more inequivalent carbon atoms, the position-specific isotope substitutions are marked in bold font. For a full list of the RPFR values see Tables S.1 and S.2.

Compound	$A \times 10^{-6}$	$B \times 10^{-5}$	$C \times 10^{-4}$	$D \times 10^{-4}$	E	$^{13}\beta$ (25 °C)	C valence
CO_2 (g)	378.971	–422.108	231.331	171.986	0.991924	1.1985	+4
CH_3-**C**OOH	355.064	–480.175	298.386	–52.862	1.001026	1.1827	+3
CH_3-**C**OSCoA	296.299	–395.606	249.130	–29.922	1.000209	1.1587	+3
CHO-MFR	360.010	–464.949	272.630	20.041	0.998523	1.1821	+2
CHO-H_4MPT	330.577	–431.111	261.215	12.120	0.998480	1.1756	+2
CH≡H_4MPT$^+$	316.709	–413.527	257.571	22.179	0.998312	1.1796	+2
CH_2=H_4MPT	204.063	–296.311	208.790	37.254	0.997932	1.1593	0
CH_3-OH	235.761	–309.752	180.321	90.980	0.996065	1.1424	–2
CH_3-H_4MPT	191.942	–257.125	164.937	97.403	0.995777	1.1413	–2
CH_3-SCoM	145.468	–194.885	127.383	111.103	0.995456	1.1209	–2
CH_3-COOH	184.170	–246.096	157.450	100.524	0.995793	1.1371	–3
CH_3-COSCoA	185.514	–247.784	158.102	101.067	0.995780	1.1375	–3
CH_4 (g)	190.098	–230.199	119.420	159.209	0.993661	1.1186	–4

Table 4: **Coefficients for the fourth-order polynomial fits to ^{13,2}RPFR values.** Computed at the M06-L/def2-TZVP level of theory, between 273.15 and 973.15 K (0-700 °C). The fit to all values is of the form $A \times 10^{12}/T^4 + B \times 10^9/T^3 + C \times 10^6/T^2 + D \times 10^3/T + E$. For compounds with steric centers, we present the relevant stereoisomers (pro-R or pro-S). For a full list of the RPFR values see Tables S.1 and S.2.

Compound	$A \times 10^{-3}$	$B \times 10^{-2}$	$C \times 10^{-2}$	$D \times 10^{-2}$	E	^{13,2}RPFR (25 °C)	C valence
CHO-MFR	276.519	–147.767	409.088	–394.266	2.596187	14.6322	+2
CHO-H_4MPT	253.624	–135.125	376.217	–359.983	2.451389	13.8121	+2
CH≡H_4MPT$^+$	295.355	–160.317	440.307	–425.042	2.717397	14.8817	+2
CH_2=H_4MPT (pro-S)	334.631	–183.173	498.905	–494.123	2.998400	15.7842	0
CH_2=H_4MPT (pro-R)	335.623	–183.769	500.478	–495.239	3.002964	15.8290	0
CH_3-OH	259.118	–136.428	382.098	–362.833	2.464551	14.5949	–2
CH_3-H_4MPT	255.130	–134.664	376.721	–356.845	2.438415	14.3256	–2
CH_3-SCoM	223.774	–116.526	330.031	–305.129	2.227630	13.4725	–2
CH_3-COOH	217.330	–112.661	320.668	–295.474	2.191095	13.3493	–3
CH_3-COSCoA	222.842	–115.969	329.053	–304.161	2.224800	13.4843	–3
CH_4 (g)	175.010	–86.612	256.157	–222.475	1.891761	12.7142	–4

Table 5: **Equilibrium carbon and hydrogen isotope fractionation factors at 25 °C, 50 °C and 75 °C.** Notations: (s) secondary isotope effects, (p) primary isotope effects, (g) gas phase, (l) liquid phase, (S) is the pro-S face, and (R) is the pro-R face of molecules with a chiral center. In the acetoclastic pathway, C_1 is the methyl bound carbon atom, and C_2 is the carboxyl or CoA bound carbon atom. The full reactions are listed in Table 1.

Enzyme	Reactant	Product	$1000\ln{}^{13}\alpha^{eq}_{r-p}$ (‰)			$1000\ln{}^{2}\alpha^{eq}_{r-p}$ (‰)		
			25 °C	50 °C	75 °C	25 °C	50 °C	75 °C
Hydrogenotrophic pathway								
Net	$CO_{2(g)}$ / $H_2O_{(l)}$	$CH_{4(g)}$	69.4	61.0	56.9	195.3	177.9	165.6
Fmd	$CO_{2(g)}$ / $H_2O_{(l)}$	CHO-MFR	13.9	13.1	12.7	110.1	109.9	111.4
Ftr	CHO-MFR	CHO-H_4MPT	5.5	5.3	5.1	51.6	48.2	45.1
Mch	CHO-H_4MPT	CH≡H_4MPT$^+$	–3.3	–2.9	–2.7	–70.5	–65.2	–61.1
Mtd (p)	$F_{420}H_2$ (S)	CH_2=H_4MPT (R)	–	–	–	–105.2	–94.0	–84.3
Mtd (s)	CH≡H_4MPT$^+$	CH_2=H_4MPT (S)	16.9	15.6	14.8	–78.2	–68.3	–59.5
Hmd	H_2	CH_2=H_4MPT (R)	–	–	–	–1359.0	–1202.1	–1069.6
Mer (p)	$F_{420}H_2$ (S)	CH_3-H_4MPT	–	–	–	–23.9	–25.8	–27.0
Mer (s)	CH_2=H_4MPT (R)	CH_3-H_4MPT	15.8	13.2	12.0	81.3	68.2	57.3
Mer (s)	CH_2=H_4MPT (S)	CH_3-H_4MPT	–	–	–	84.0	71.0	60.2
Mtr	CH_3-H_4MPT	CH_3-SCoM	18.1	15.9	14.9	42.9	38.2	34.1
Mcr (p)	HS-CoB	$CH_{4(g)}$	–	–	–	–635.8	–580.0	–531.6
Mcr (s)	CH_3-SCoM	$CH_{4(g)}$	2.1	0.8	0.2	55.4	44.2	35.3
Acetoclastic pathway								
Net	CH_3-COO^- (C_1)	$CH_{4(g)}$	15.7	13.5	12.1	31.9	23.6	17.2
Net	CH_3-COO^- (C_2)	$CO_{2(g)}$ / $H_2O_{(l)}$	–13.3	–13.4	–13.5	–162.1	–153.7	–147.4
Ack/Pta	CH_3-COO^- (C_1)	CH_3-COSCoA (C_1)	–0.4	–0.4	–0.3	–9.4	–8.5	–7.7
Cdh	CH_3-COSCoA (C_1)	CH_3-H_4MPT	–3.2	–2.8	–2.6	–57.0	–50.2	–44.5
Methylotrophic pathway								
Net	CH_3OH	$CH_{4(g)}$	20.3	18.0	16.5	115.8	98.9	85.0
Net	CH_3OH	$CO_{2(g)}$ / $H_2O_{(l)}$	–46.7	–42.9	–40.4	–79.3	–79.1	–81.0
Mta	CH_3OH	CH_3-SCoM	18.6	17.2	16.3	60.4	54.8	49.7
Electron cycling								
Frh	$H_2O_{(l)}$	$F_{420}H_2$ (S)	–	–	–	120.9	121.4	123.2
Hdr	$H_2O_{(l)}$	HS-CoB	–	–	–	831.1	757.9	697.2

Table 6: **Carbon isotopic fractionation during AOM.** The maximum net CH_4–CO_2 carbon isotope fractionation ($1000\ln^{13}\alpha_{CH_4-CO_2}$) that can be obtained at a steady state, when a single reaction is irreversible ($f = 0$) and all other reactions remain completely reversible ($f = 1$), using the framework outlined in Appendix A. We used the experimentally-determined KFF of Mcr ($1000\ln^{13}\alpha^{kin}_{CH_4\rightarrow CH_3\text{-}SCoM}$ = 38 ‰; Scheller et al., 2013). The KFFs of the other enzymes were uniformly assigned values of 5‰ or 40‰.

	$1000\ln^{13}\alpha_{CH_4-CO_2}$	
Irreversible reaction	$1000\ln^{13}\alpha^{kin}$ = 5‰	$1000\ln^{13}\alpha^{kin}$ = 40‰
Mcr	37.9	37.9
Mtr	3.0	37.9
Mer	–14.0	20.0
Mtd	–30.6	4.4
Mch	–47.8	–12.7
Ftr	–44.4	–9.3
Fmd	–49.9	–14.8

Table 7: **Scenarios of reversibility control over the net carbon isotopic fractionation in the considered pathways.** In all scenarios, the reversibility f (defined as the ratio of the backward and forward fluxes) of each enzymatically catalyzed reaction ranges from 1 (i.e., fully reversible) to 0 (i.e., irreversible). References are to previous reports that used the scenario.

Scenario description	**Ref.**	**1000ln$^{13}\alpha$**
Hydrogenotrophic pathway (Section 4.4.1)		
(*i*) Uniform departure from equilibrium of all reactions ($f = 1 \rightarrow 0$).	1	20‰ to 69‰
(*ii*) Equilibrium between CO_2 and CH_3-SCoM ($f = 1$), gradual departure from equilibrium of the Mcr-catalyzed reaction ($f = 1 \rightarrow 0$).	2, 3	69‰ to 106‰
(*iii*) Pathway reduced to four carbon reduction steps (Fmd, Mtd, Mer, Mcr), with f of either 0 or 1 for each.	4	20‰ to 106‰
Methylotrophic pathway (Section 4.4.3)		
Variable reversibility between CH_3OH and CH_3-SCoM, and between CH_3-SCoM and CH_4 (f drawn from a uniform distribution between 0 and 1). Between CH_3-SCoM and CO_2 f is set to 0.75.	–	Depends on $R_{r/o}$, the reduction:oxidation ratio of methanol
Acetoclastic pathway (Section 4.4.4)		
Equilibrium between CH_3-COO^- and CH_3-SCoM ($f = 1$), gradual departure from equilibrium of the Mcr-catalyzed reaction ($f = 1 \rightarrow 0$).	–	16‰ to 53‰
AOM (Section 4.4.5)		
All reactions are fully reversible ($f = 1$), with the exception of a single reaction that is irreversible ($f = 0$). The identity of the irreversible reaction is varied to produce the range.	2	–69‰ to 37‰

(1) Wang et al. (2015); (2) Alperin & Hoehler (2009); (3) Stolper et al. (2015); (4) Cao et al. (2019).

7 FIGURES

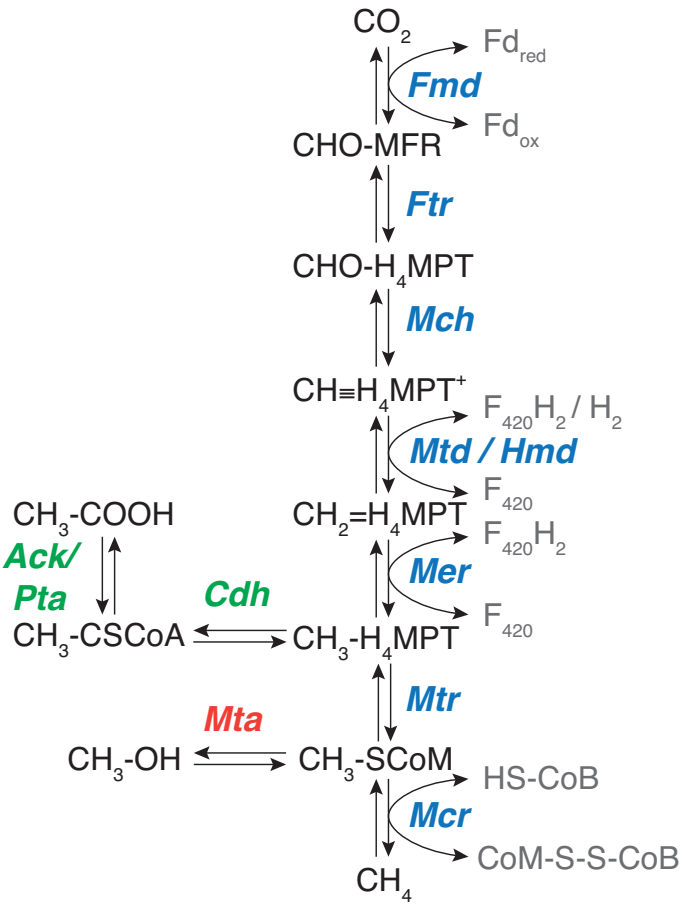

Figure 1: **Metabolic pathways of methanogenesis and anaerobic oxidation of methane (AOM).** The metabolite names are in black, electron carriers in gray, and enzymes in bold-italicized colored fonts. The reactions that are unique to the acetoclastic and methylotrophic pathways are in green and red, respectively. The reactions in blue are the hydrogenotrophic and AOM pathways, and are common also with the acetoclastic and methylotrophic pathways. All the reactions are assumed to have the potential for full reversibility.

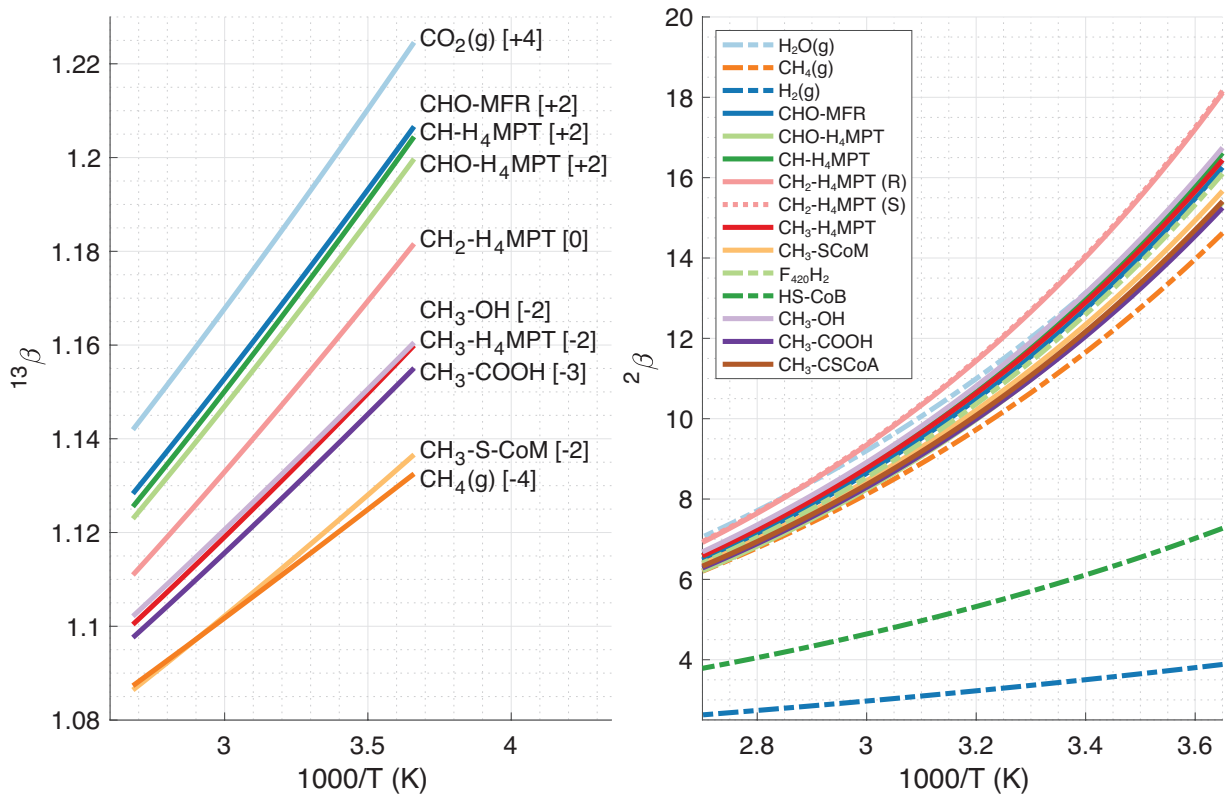

Figure 2: **Calculated carbon (left) and hydrogen (right) β values.** The carbon oxidation state is given in square brackets. (R) and (S) indicate the pro-R and pro-S faces of chiral CH_2-H_4MPT.

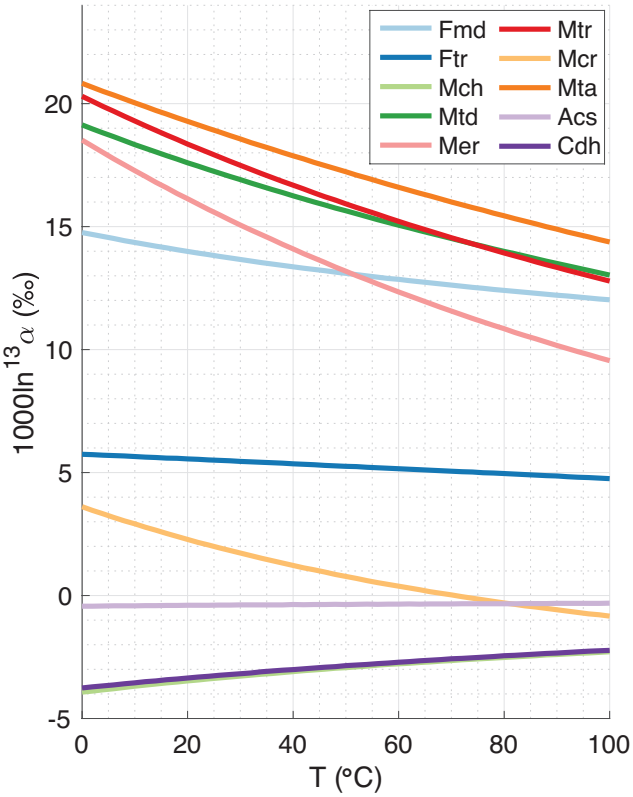

Figure 3: **Temperature dependence of the calculated equilibrium carbon isotope fractionation factors (EFFs) for the reactions involved in methanogenesis.** The reactions catalyzed by the enzymes shown in the figure legend are listed in Table 1.

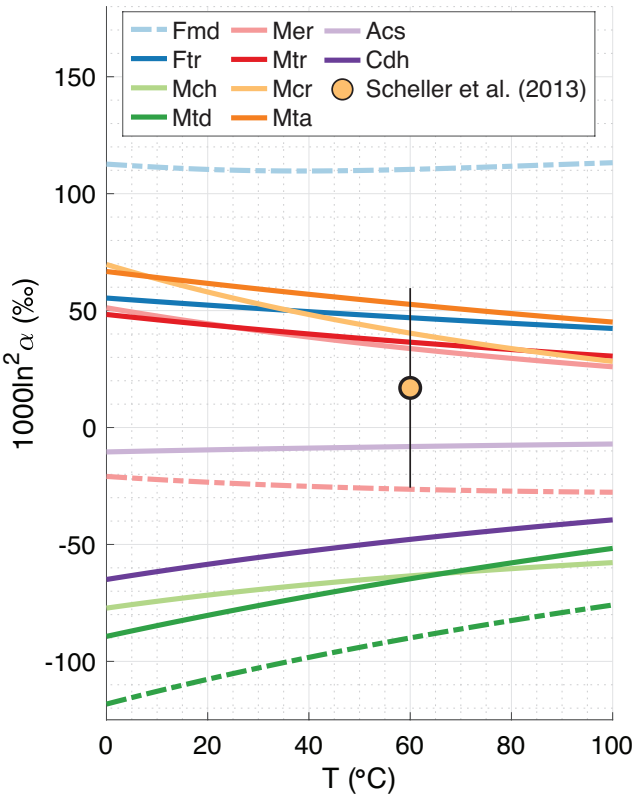

Figure 4: **Temperature dependence of the calculated equilibrium hydrogen isotope fractionation factors (EFFs) for the reactions involved in methanogenesis.** The dashed lines represent primary EFFs, and the solid lines represent secondary EFFs. The orange circle is a measurement of $1000\ln^2\alpha^{\mathrm{eq}}_{\mathrm{CH_3\text{-}SCoM-CH_4}}$ for the reaction catalyzed by Mcr (Scheller et al., 2013) with the respective error bars.

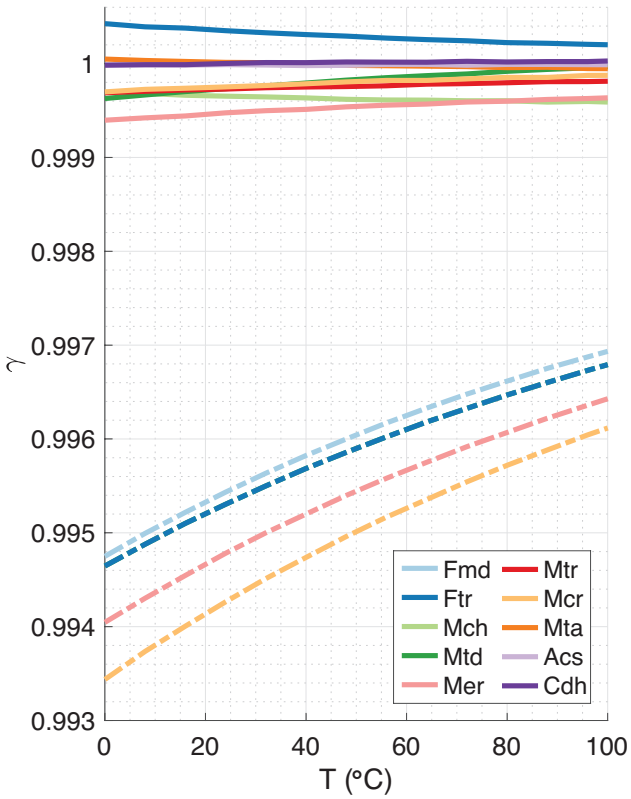

Figure 5: **Temperature dependence of the clumped isotopologue equilibrium fractionation factors (EFFs).** The EFFs are expressed as γ, where $\gamma = {}^{13,2}\alpha / \left({}^{13}\alpha \times {}^{2}\alpha\right)$, and ${}^{13}\alpha$ and ${}^{2}\alpha$ are the carbon and hydrogen EFFs, respectively. The dashed and solid lines are γ for primary and secondary EFFs, respectively.

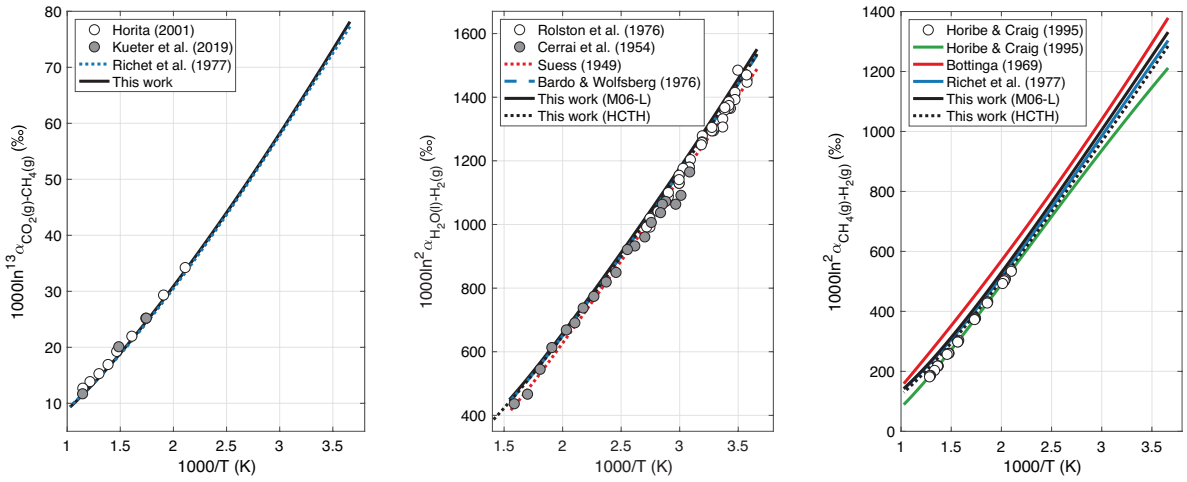

Figure 6: **Comparisons of isotope fractionations calculated in this study with theoretical (lines) and experimental (circles) estimates.** *Left:* $CO_{2(g)}$–$CH_{4(g)}$ carbon isotope fractionations. *Middle:* $H_2O_{(l)}$–H_2 hydrogen isotope fractionations. *Right:* CH_4–H_2 hydrogen isotope fractionations. The green line was derived from a linear regression of ${}^2\alpha_{CH_4-H_2O}$ on $10^6/T^2$.

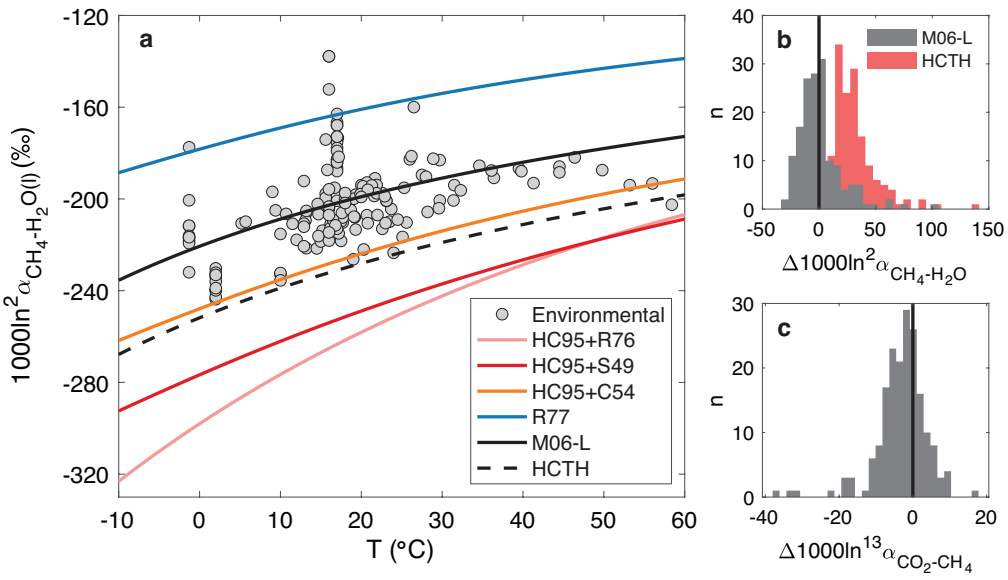

Figure 7: **Comparison of CH_4–$H_2O_{(l)}$ carbon and hydrogen isotope fractionations calculated in this and previous studies with environmental estimates.** (a) $1000\ln^2\alpha_{CH_4-H_2O}$ from theoretical studies and biogenic environmental samples. The lines were generated from different combinations of fits to experimental and theoretical work (Suess, 1949 (S49); Cerrai et al., 1954 (C54); Bottinga, 1969 (B69); Rolston et al., 1976 (R76); Richet et al., 1977 (R77); Horibe and Craig, 1995 (HC95) and this work using the M06-L and HCTH functionals). The $H_2O_{(l)}$–$H_2O_{(g)}$ hydrogen isotope fractionations were based on Horita & Wesolowski (1994), except for the results of Rolston et al. (1976), in which case this is noted in the figure legend. (b) The deviation of environmental $1000\ln^2\alpha_{CH_4-H_2O}$ from the temperature-dependent EFFs calculated in this study with the M06-L and HCTH functionals. (c) The deviation of environmental $1000\ln^{13}\alpha_{CO_2-CH_4}$ from the temperature-dependent EFFs calculated in this study with the M06-L functional. A full list of the environmental samples presented in this figure is available in Table S.3 with the corresponding references.

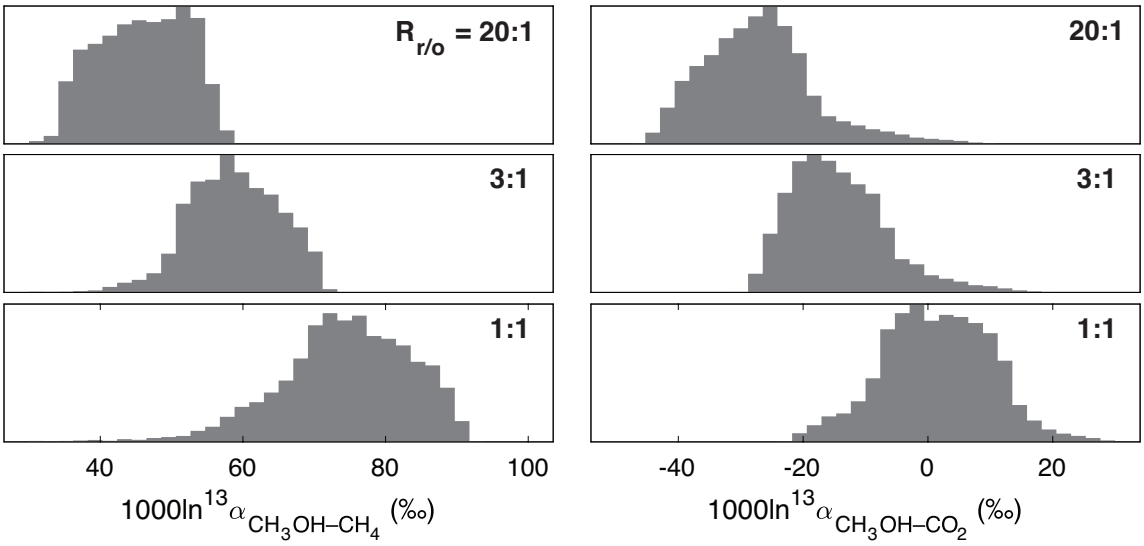

Figure 8: **Carbon isotope fractionation between methanol, CH_4 and CO_2.** *Left:* Methanol–CH_4 carbon isotope fractionation; *Right:* Methanol–CO_2 carbon isotope fractionation. Each histogram represents 10,000 simulations of methylotrophic methanogenesis with KFFs $1000\ln{}^{13}\alpha^{\text{kin}}_{\text{methanol}\rightarrow\text{CH}_3\text{-SCoM}}$ and $1000{}^{13}\alpha^{\text{kin}}_{\text{CH}_3\text{-SCoM}\rightarrow\text{CO}_2}$ in the range 30-50‰and the reversibilities between methanol and CH_3-SCoM and between CH_3-SCoM and CH_4 in the range 10^{-3} to 1, each drawn randomly from uniform distributions. The reversibility between CH_3-SCoM and CO_2 was held constant at 0.75, and the KFF $1000\ln{}^{13}\alpha^{\text{kin}}_{\text{CH}_3\text{-SCoM}\rightarrow\text{CH}_4}$ was set to 40‰ (Scheller et al., 2013). The methanol reduction:oxidation ratio, $R_{r/o}$, used for each set of simulations is indicated.

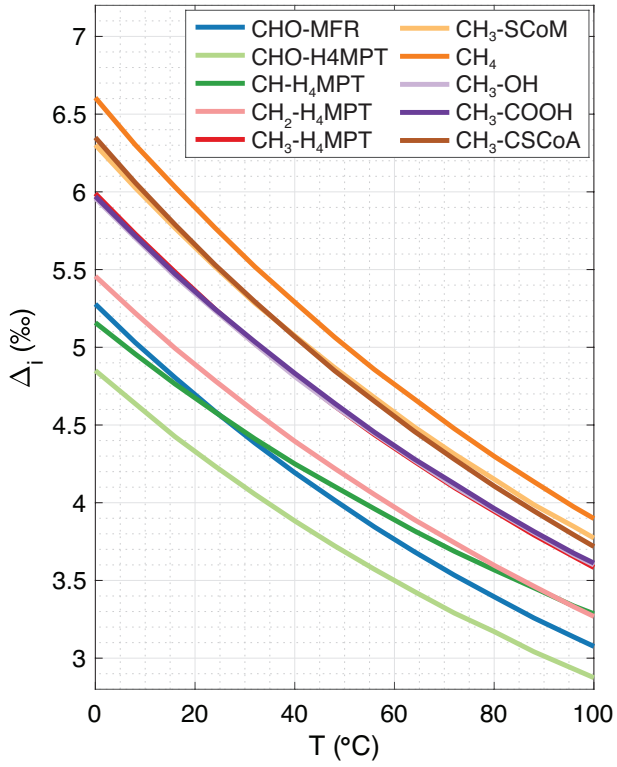

Figure S.1: **Doubly-substituted ("clumped") isotopologue compositions in methanogenesis.** The deviation of the abundance of the ^{13}C-D clumped isotopologue from the stochastic distribution is expressed as $\Delta_i = (R_i/R_i^*) - 1$, where R_i is the calculated ratio of the doubly-substituted isotopologue to the unsubstituted isotopologue, and R_i^* is this ratio at a stochastic distribution of the rare isotopes.

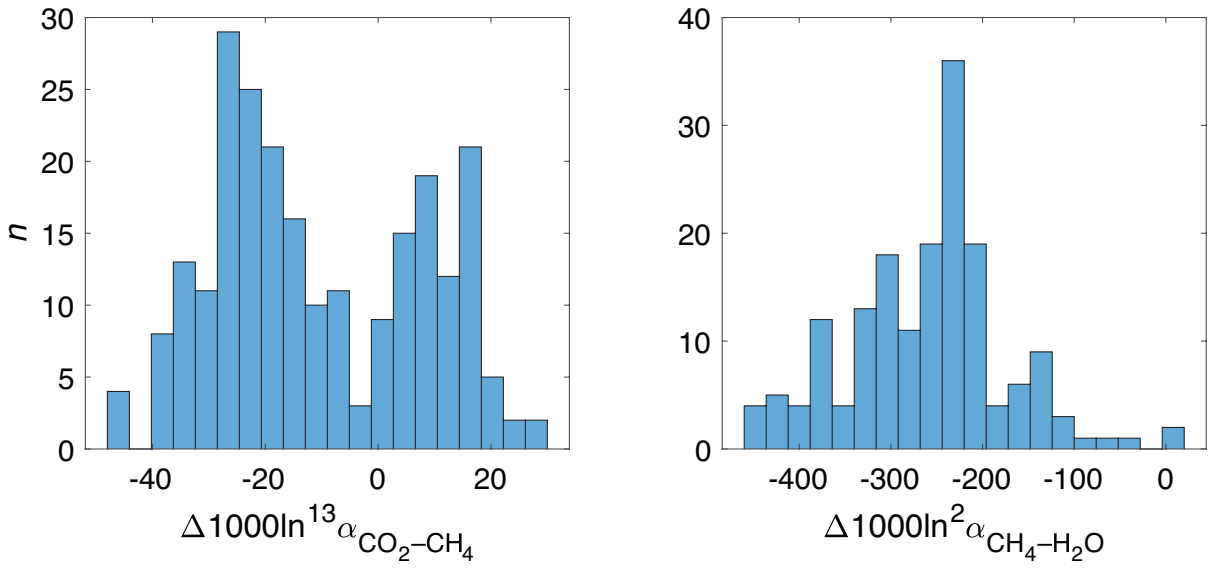

Figure S.2: **Deviations from the expected temperature-dependent EFFs in laboratory culture experiments.** *Left:* carbon isotopes ($n = 213$); *Right:* hydrogen isotopes ($n = 172$). n represents the number of samples in each bin. Laboratory data are from Valentine et al. (2004); Penning et al. (2005); Hattori et al. (2012); Okumura et al. (2016); Topçuoğlu et al. (2019). The complete list of samples is available in Table S.4.

A Isotope fractionation in linear metabolic reaction networks

A.1 General derivation

The net isotopic fractionation of any linear metabolic pathway at steady state can be described by a recursive mass balance expression, which requires knowledge of the intermediate reactions' EFFs, forward KFFs and reversibilities, where the reversibility f is defined as the ratio of the reverse and forward mass fluxes (Wing & Halevy, 2014). We implement here this recursive term for carbon isotopes in the hydrogenotrophic and AOM pathways. Under steady-state conditions, the net fractionation of the general reaction $r \rightleftarrows p$ can be described by:

$$\alpha^{\text{net}}_{r-p} = \left(\alpha^{\text{eq}}_{r-p} - \alpha^{\text{kin}}_{r\to p}\right) f_{p,r} + \alpha^{\text{kin}}_{r\to p}, \tag{A.1}$$

where α^{eq}_{r-p}, $\alpha^{\text{kin}}_{r\to p}$ and $\alpha^{\text{net}}_{r-p}$ are, respectively, the EFF between r and p, the KFF between r and the flux of r to p, and the net isotope fractionation between r and p. This treatment can be applied to linear pathways, such as $s \rightleftarrows r \rightleftarrows p$, by extending Eq. A.1:

$$\alpha^{\text{net}}_{s-p} = \left(\alpha^{\text{net}}_{r-p} \times \alpha^{\text{eq}}_{s-r} - \alpha^{\text{kin}}_{s\to r}\right) f_{r,s} + \alpha^{\text{kin}}_{s\to r} \tag{A.2}$$

(full derivation in Wing and Halevy (2014)). Eq. A.2 can be further extended by recursion to any number of reactions in a linear metabolic network at steady state. We use this type of recursive expression to explore carbon isotope fractionation in the hydrogenotrophic (Section 4.4.1)and acetoclastic (Section 4.4.4) methanogenesis, and anaerobic methane oxidation (Section 4.4.5) pathways.

A.2 Equations for hydrogenotrophic methanogenesis and AOM

We used Eqs. A.3–A.9 to calculate the net carbon isotope fractionation at steady state between (*i*) CO_2 and CH_4 (Section 4.4.1) and (*ii*) CH_4 and CO_2 (Section 4.4.5). For brevity, we denote here the molecules in the pathway by the letters A-H, where for case (*i*) A is CO_2 and H is CH_4, with the intracellular carbon-bearing molecules denoted by B-G, and for case (*ii*) we use the reverse

notation where CH_4 is A and CO_2 is H.

$$\alpha^{\text{net}}_{\text{G}-\text{H}} = \left(\alpha^{\text{eq}}_{\text{G}-\text{H}} - \alpha^{\text{kin}}_{\text{G}\to\text{H}}\right) f_{\text{H,G}} + \alpha^{\text{kin}}_{\text{G}\to\text{H}} \tag{A.3}$$

$$\alpha^{\text{net}}_{\text{F}-\text{H}} = \left(\alpha^{\text{net}}_{\text{G}-\text{H}} \times \alpha^{\text{eq}}_{\text{F}-\text{G}} - \alpha^{\text{kin}}_{\text{F}\to\text{G}}\right) f_{\text{G,F}} + \alpha^{\text{kin}}_{\text{F}\to\text{G}} \tag{A.4}$$

$$\alpha^{\text{net}}_{\text{E}-\text{H}} = \left(\alpha^{\text{net}}_{\text{F}-\text{H}} \times \alpha^{\text{eq}}_{\text{E}-\text{F}} - \alpha^{\text{kin}}_{\text{E}\to\text{F}}\right) f_{\text{F,E}} + \alpha^{\text{kin}}_{\text{E}\to\text{F}} \tag{A.5}$$

$$\alpha^{\text{net}}_{\text{D}-\text{H}} = \left(\alpha^{\text{net}}_{\text{E}-\text{H}} \times \alpha^{\text{eq}}_{\text{D}-\text{E}} - \alpha^{\text{kin}}_{\text{D}\to\text{E}}\right) f_{\text{E,D}} + \alpha^{\text{kin}}_{\text{D}\to\text{E}} \tag{A.6}$$

$$\alpha^{\text{net}}_{\text{C}-\text{H}} = \left(\alpha^{\text{net}}_{\text{D}-\text{H}} \times \alpha^{\text{eq}}_{\text{C}-\text{D}} - \alpha^{\text{kin}}_{\text{C}\to\text{D}}\right) f_{\text{D,C}} + \alpha^{\text{kin}}_{\text{C}\to\text{D}} \tag{A.7}$$

$$\alpha^{\text{net}}_{\text{B}-\text{H}} = \left(\alpha^{\text{net}}_{\text{C}-\text{H}} \times \alpha^{\text{eq}}_{\text{B}-\text{C}} - \alpha^{\text{kin}}_{\text{B}\to\text{C}}\right) f_{\text{C,B}} + \alpha^{\text{kin}}_{\text{B}\to\text{C}} \tag{A.8}$$

$$\alpha^{\text{net}}_{\text{A}-\text{H}} = \left(\alpha^{\text{net}}_{\text{B}-\text{H}} \times \alpha^{\text{eq}}_{\text{A}-\text{B}} - \alpha^{\text{kin}}_{\text{A}\to\text{B}}\right) f_{\text{B,A}} + \alpha^{\text{kin}}_{\text{A}\to\text{B}} \tag{A.9}$$

B Isotope fractionation in nonlinear metabolic reaction networks

The analytical expression for the calculation of net isotope fractionation presented in Appendix A is only applicable to reversible, linear networks. However, if some of the reactions in the network have more than one source of the atom of interest, an analytical solution is usually not possible, and a numerical solution is required. Consider the reaction:

$$a\mathrm{Y}_n + b\mathrm{Y}_m \underset{\phi_{\mathrm{pr}}}{\overset{\phi_{\mathrm{rp}}}{\rightleftharpoons}} c\mathrm{Y}_{(n+m)} \tag{B.1}$$

where a, b and c are are arbitrary organic residues, Y is the atom of interest, n and m are the stoichiometric coefficients of Y, and ϕ is the reaction flux. For brevity, we denote $a\mathrm{Y}_n$, $b\mathrm{Y}_m$ and $c\mathrm{Y}_{(n+m)}$ as r_1, r_2 and p, respectively. The change of the isotopic composition of compound p with time is:

$$\frac{d}{dt}R_p = \frac{1}{[p]}\Big[\phi_{rp}\left(n\cdot\alpha^{\mathrm{kin}}_{r_1\to p}R_{r_1} + m\cdot\alpha^{\mathrm{kin}}_{r_2\to p}R_{r_2}\right) - \phi_{pr}\cdot R_p\left(n\cdot\alpha^{\mathrm{kin}}_{p\to r_1} + m\cdot\alpha^{\mathrm{kin}}_{p\to r_2}\right) - R_p(m+n)\left(\phi_{rp}-\phi_{pr}\right)\Big], \tag{B.2}$$

where R_{r_1}, R_{r_2} and R_p are the ratios of the rare to abundant isotopes in pools r_1, r_2 and p, respectively. In the specific case of a chemical and isotopic steady state, the concentration and isotopic composition of p are constant, and $\frac{dR_p}{dt} = \frac{d[p]}{dt} = 0$. Rearranging Eq. B.2 yields an analytical solution for R_p at steady state:

$$R_p = \frac{\phi_{rp}\left(n\cdot\alpha^{\mathrm{kin}}_{r_1\to p}R_{r_1} + m\cdot\alpha^{\mathrm{kin}}_{r_2\to p}R_{r_2}\right)}{\phi_{pr}\left(n\cdot\alpha^{\mathrm{kin}}_{p\to r_1} + m\cdot\alpha^{\mathrm{kin}}_{p\to r_2}\right) + (m+n)\left(\phi_{rp}-\phi_{pr}\right)} \tag{B.3}$$

(Full derivation in Eq. S5 in Wing and Halevy (2014)). This approach is used here for two specific cases: hydrogen isotope fractionation in hydrogenotrophic methanogenesis (Section 4.4.2) and carbon isotope fractionation in methylotrophic methanogenesis (Section 4.4.3).

B.1 Hydrogen isotope fractionation in the hydrogenotrophic methanogenesis pathway

The last reaction in the hydrogenotrophic methanogenesis pathway, catalyzed by Mcr, has a large negative $\Delta\mathrm{G}^0_\mathrm{r}$ ($\sim$–30 kJ mol^{-1} at 25 °C) and is thought to be practically irreversible during methanogenesis (i.e., $\phi_{\mathrm{CH_3\text{-}SCoM}\to\mathrm{CH_4}} \ggg \phi_{\mathrm{CH_4}\to\mathrm{CH_3\text{-}SCoM}}$) (Thauer, 2011). In this case, the reverse reactions from methane will not affect the net isotope composition, and Eq. B.3 can be simplified to:

$${}^2R_{\mathrm{CH_4}} = \frac{3}{4}\times{}^2\alpha^{\mathrm{kin}}_{\mathrm{CH_3\text{-}SCoM}\to\mathrm{CH_4}}{}^2R_{\mathrm{CH_3\text{-}SCoM}} + \frac{1}{4}\times{}^2\alpha^{\mathrm{kin}}_{\mathrm{HS\text{-}CoB}\to\mathrm{CH_4}}{}^2R_{\mathrm{HS\text{-}CoB}}. \tag{B.4}$$

In the specific case that the reaction between H_2O and CH_3-SCoM, and coenzyme B reduction to HS-CoB are at chemical and isotopic equilibrium, then:

$$^2R_{\text{CH}_3\text{-SCoM}} = {}^2R_{\text{H}_2\text{O}} / {}^2\alpha^{\text{eq}}_{\text{H}_2\text{O}-\text{CH}_3\text{-SCoM}} \tag{B.5}$$

and

$$^2R_{\text{HS-CoB}} = {}^2R_{\text{H}_2\text{O}} / {}^2\alpha^{\text{eq}}_{\text{H}_2\text{O}-\text{HS-CoB}}. \tag{B.6}$$

Eq. B.4 is then:

$$^2R_{\text{CH}_4} = \frac{3}{4}\left(\alpha^{\text{kin}}_{\text{CH}_3\text{-SCoM}\rightarrow\text{CH}_4} \cdot {}^2R_{\text{H}_2\text{O}} / {}^2\alpha^{\text{eq}}_{\text{H}_2\text{O}-\text{CH}_3\text{-SCoM}}\right) + \frac{1}{4}\left({}^2\alpha^{\text{kin}}_{\text{HS-CoB}\rightarrow\text{CH}_4} \cdot {}^2R_{\text{H}_2\text{O}} / {}^2\alpha^{\text{eq}}_{\text{H}_2\text{O}-\text{HS-CoB}}\right). \tag{B.7}$$

The net hydrogen isotope fractionation between CH_4 and H_2O, ${}^2\alpha_{\text{CH}_4-\text{H}_2\text{O}}$, can be calculated by dividing both sides of Eq. B.7 by ${}^2R_{\text{H}_2\text{O}}$:

$$^2\alpha_{\text{CH}_4-\text{H}_2\text{O}} = \frac{3}{4}\left({}^2\alpha^{\text{kin}}_{\text{CH}_3\text{-SCoM}\rightarrow\text{CH}_4} / {}^2\alpha^{\text{eq}}_{\text{H}_2\text{O}-\text{CH}_3\text{-SCoM}}\right) + \frac{1}{4}\left({}^2\alpha^{\text{kin}}_{\text{HS-CoB}\rightarrow\text{CH}_4} / {}^2\alpha^{\text{eq}}_{\text{H}_2\text{O}-\text{HS-CoB}}\right). \tag{B.8}$$

B.2 Carbon isotope fractionation in the methylotrophic methanogenesis pathway

In the methylotrophic methanogenesis pathway, methanol is converted to CH_3-SCoM, which is then either oxidized to CO_2 in the reverse methanogenic pathway or reduced to CH_4 by the Mcr-catalyzed reaction (Fig. 1):

$$(n+m)\cdot\text{CH}_3\text{OH} \rightleftarrows (n+m)\cdot\text{CH}_3\text{-S-CoM} \rightleftarrows n\cdot\text{CH}_4 + m\cdot\text{CO}_2, \tag{B.9}$$

where n and m are stoichiometric coefficients. This is a simplified view of the pathway, yet it includes the pathway's three main branches. We define $R_{r/o} \equiv n:m$, the ratio of the reduced and oxidized branches. If all methanol molecules are converted to either CO_2 or CH_4, $R_{r/o}$ is expected to be 3:1, as the source of the 2 electrons for CH_3-SCoM reduction to CH_4 is from the full oxidation of CH_3-SCoM to CO_2, which yields 6 electrons. However, if some of the CH_3-SCoM is instead converted to biomass, $R_{r/o}$ may vary. For brevity, we denote the metabolites here as A (CH_3OH), B (CH_3-SCoM), C (CH_4) and D (CO_2). The change in the isotopic composition of B (R_B) with time is:

$$\begin{aligned}\frac{d}{dt}{}^{13}R_{\text{B}} = \frac{1}{[\text{B}]}\Big[&(n+m)\cdot\phi_{\text{AB}}\,{}^{13}\alpha^{\text{kin}}_{\text{A}\rightarrow\text{B}}\,{}^{13}R_{\text{A}} + n\cdot\phi_{\text{CB}}\,{}^{13}\alpha^{\text{kin}}_{\text{C}\rightarrow\text{B}}\,{}^{13}R_{\text{C}} + m\cdot\phi_{\text{DB}}\,{}^{13}\alpha^{\text{kin}}_{\text{D}\rightarrow\text{B}}\,{}^{13}R_{\text{D}} - \\ &{}^{13}R_{\text{B}}\left((n+m)\cdot\phi_{\text{BA}}\,{}^{13}\alpha^{\text{kin}}_{\text{B}\rightarrow\text{A}} + n\cdot\phi_{\text{BC}}\,{}^{13}\alpha^{\text{kin}}_{\text{B}\rightarrow\text{C}} + m\cdot\phi_{\text{BD}}\,{}^{13}\alpha^{\text{kin}}_{\text{B}\rightarrow\text{D}}\right) - \\ &{}^{13}R_{\text{B}}\Big((n+m)(\phi_{\text{AB}}-\phi_{\text{BA}}) + n(\phi_{\text{CB}}-\phi_{\text{BC}}) + m(\phi_{\text{DB}}-\phi_{\text{BD}})\Big)\Big].\end{aligned} \tag{B.10}$$

We write similar time derivatives for C and D:

$$\frac{d}{dt}{}^{13}R_{\mathrm{C}} = \frac{1}{[\mathrm{C}]} \cdot n \left[\phi_{\mathrm{BC}} {}^{13}\alpha^{\mathrm{kin}}_{\mathrm{B}\to\mathrm{C}} {}^{13}R_{\mathrm{B}} - \phi_{\mathrm{CB}} {}^{13}\alpha^{\mathrm{kin}}_{\mathrm{C}\to\mathrm{B}} {}^{13}R_{\mathrm{C}} - {}^{13}R_{\mathrm{C}} \left(\phi_{\mathrm{BC}} - \phi_{\mathrm{CB}}\right) \right], \tag{B.11}$$

$$\frac{d}{dt}{}^{13}R_{\mathrm{D}} = \frac{1}{[\mathrm{D}]} \cdot m \left[\phi_{\mathrm{BD}} {}^{13}\alpha^{\mathrm{kin}}_{\mathrm{B}\to\mathrm{D}} {}^{13}R_{\mathrm{B}} - \phi_{\mathrm{DB}} {}^{13}\alpha^{\mathrm{kin}}_{\mathrm{D}\to\mathrm{B}} {}^{13}R_{\mathrm{D}} - {}^{13}R_{\mathrm{D}} \left(\phi_{\mathrm{BD}} - \phi_{\mathrm{DB}}\right) \right]. \tag{B.12}$$

The metabolic network of the methyltrophic pathway as presnted in Eq. B.9 is non-linear. Thus, the isotope fractionations between A, C and D are not independent of each other, and an analytical solution is nontrivial and provides little intuition. Instead, a numerical solution to this system is possible, by forward integration of Eqs. B.10–B.12 until the steady-state solution is obtained. To solve this systen, we used the ode15s solver in MATLAB®. We assigned the reversibility of the reactions (f), the net rate (ϕ_{net}), ${}^{13}R_{\mathrm{A}}$, and the forward KFFs ${}^{13}\alpha^{\mathrm{kin}}$. We calculated the backward KFFs by the relation $\alpha^{\mathrm{eq}}_{\mathrm{A-B}} = \alpha^{\mathrm{kin}}_{\mathrm{B}\to\mathrm{A}} / \alpha^{\mathrm{kin}}_{\mathrm{A}\to\mathrm{B}}$. We assumed that the reaction from CH_3-SCoM to CO_2 is partially reversible, i.e., $\phi_{\mathrm{DB}}/\phi_{\mathrm{BD}} = 0.75$, to obtain the ideal fit to the observed ranges of methanol–CH_4 and methanol–CO_2 carbon isotope fractionations. The forward and reverse fluxes are related to the net rate and the fs:

$$\phi_{\mathrm{AB}} = \frac{\phi_{net}}{1 - f_{\mathrm{B,A}}}, \tag{B.13}$$

$$\phi_{\mathrm{BA}} = \frac{\phi_{net} \times f_{\mathrm{B,A}}}{1 - f_{\mathrm{B,A}}}. \tag{B.14}$$

References

Alperin, M. J., & Hoehler, T. M. (2009). Anaerobic methane oxidation by archaea/sulfate-reducing bacteria aggregates: 2. Isotopic constraints. *American Journal of Science*, **309**, 958–984. doi:10.2475/10.2009.02.

Alstad, K. P., & Whiticar, M. J. (2011). Carbon and hydrogen isotope ratio characterization of methane dynamics for Fluxnet Peatland Ecosystems. *Organic Geochemistry*, **42**, 548–558. doi:10.1016/j.orggeochem.2011.03.004.

Andrae, D., Häuß ermann, U., Dolg, M., Stoll, H., & Preuß, H. (1990). Energy-adjustedab initio pseudopotentials for the second and third row transition elements. *Theoretica chimica acta*, **77**, 123–141. doi:10.1007/BF01114537.

Bardo, R. D., & Wolfsberg, M. (1976). A theoretical calculation of the equilibrium constant for the isotopic exchange reaction between water and hydrogen deuteride. *The Journal of Physical Chemistry*, **80**, 1068–1071. doi:10.1021/j100551a009.

Berghuis, B. A., Yu, F. B., Schulz, F., Blainey, P. C., Woyke, T., & Quake, S. R. (2019). Hydrogenotrophic methanogenesis in archaeal phylum Verstraetearchaeota reveals the shared ancestry of all methanogens. *Proceedings of the National Academy of Sciences*, **116**, 5037–5044. doi:10.1073/pnas.1815631116.

Bigeleisen, J., & Mayer, M. G. (1947). Calculation of Equilibrium Constants for Isotopic Exchange Reactions. *The Journal of Chemical Physics*, **15**, 261–267. doi:10.1063/1.1746492.

Black, J. R., Yin, Q.-z., Rustad, J. R., & Casey, W. H. (2007). Magnesium Isotopic Equilibrium in Chlorophylls. *Journal of the American Chemical Society*, **129**, 8690–8691. doi:10.1021/JA072573I.

Boese, A. D., & Handy, N. C. (2001). A new parametrization of exchange–correlation generalized gradient approximation functionals. *The Journal of Chemical Physics*, **114**, 5497–5503. doi:10.1063/1.1347371.

Bottinga, Y. (1969). Calculated fractionation factors for carbon and hydrogen isotope exchange in the system calcite-carbon dioxide-graphite-methane-hydrogen-water vapor. *Geochimica et Cosmochimica Acta*, **33**, 49–64. doi:10.1016/0016-7037(69)90092-1.

Cao, X., Bao, H., & Peng, Y. (2019). A kinetic model for isotopologue signatures of methane generated by biotic and abiotic CO2 methanation. *Geochimica et Cosmochimica Acta*, **249**, 59–75. doi:10.1016/J.GCA.2019.01.021.

Cao, X., & Liu, Y. (2012). Theoretical estimation of the equilibrium distribution of clumped isotopes in nature. *Geochimica et Cosmochimica Acta*, **77**, 292–303. doi:10.1016/j.gca.2011.11.021.

Cerrai, E., Marchetti, C., Renzoni, R., Roseo, L., Silvesti, M., & Villari, S. (1954). A Thermal Method for Concentrating Heavy Water. In *Chem. Eng. Prog. Symp* (pp. 271–280). volume 50.

Chuang, P.-C., Frank Yang, T., Wallmann, K., Matsumoto, R., Hu, C.-Y., Chen, H.-W., Lin, S., Sun, C.-H., Li, H.-C., Wang, Y., & Dale, A. W. (2018). Carbon isotope exchange during anaerobic oxidation of methane (AOM) in sediments of the northeastern South China Sea. *Geochimica et Cosmochimica Acta*, **246**, 138–155. doi:10.1016/J.GCA.2018.11.003.

DePaolo, D. J. (2011). Surface kinetic model for isotopic and trace element fractionation during precipitation of calcite from aqueous solutions. *Geochimica et Cosmochimica Acta*, **75**, 1039–1056. doi:10.1016/j.gca.2010.11.020.

Domagal-Goldman, S. D., & Kubicki, J. D. (2008). Density functional theory predictions of equilibrium isotope fractionation of iron due to redox changes and organic complexation. *Geochimica et Cosmochimica Acta*, **72**, 5201–5216. doi:10.1016/j.gca.2008.05.066.

Egger, M., Riedinger, N., Mogollón, J. M., & Jø rgensen, B. B. (2018). Global diffusive fluxes of methane in marine sediments. *Nature Geoscience*, **11**, 421–425. doi:10.1038/s41561-018-0122-8.

Eldridge, D., Guo, W., & Farquhar, J. (2016). Theoretical estimates of equilibrium sulfur isotope effects in aqueous sulfur systems: Highlighting the role of isomers in the sulfite and sulfoxylate systems. *Geochimica et Cosmochimica Acta*, **195**, 171–200. doi:10.1016/J.GCA.2016.09.021.

Eldridge, D. L., Korol, R., Lloyd, M. K., Turner, A. C., Webb, M. A., Miller, T. F., & Stolper, D. (2019). Comparison of Experimental vs. Theoretical Abundances of 13CH3D and 12CH2D2 for Isotopically Equilibrated Systems From 1-500°C. *ACS Earth and Space Chemistry*, **3**, 2747–2764. doi:10.1021/acsearthspacechem.9b00244.

Frisch, M., Trucks, G., Schlegel, H., Scuseria, G., Robb, M., Cheeseman, J., Scalmani, G., Barone, V., Petersson, G., Nakatsuji, H. et al. (2016). Gaussian 16. *Revision A*, **3**.

Fujii, T., Moynier, F., Blichert-Toft, J., & Albarède, F. (2014). Density functional theory estimation of isotope fractionation of Fe, Ni, Cu, and Zn among species relevant to geochemical and biological environments. *Geochimica et Cosmochimica Acta*, **140**, 553–576. doi:10.1016/J.GCA.2014.05.051.

Galimov, E. (2006). Isotope organic geochemistry. *Organic Geochemistry*, **37**, 1200–1262. doi:10.1016/j.orggeochem.2006.04.009.

Gelwicks, J. T., Risatti, J. B., & Hayes, J. M. (1994). Carbon isotope effects associated with aceticlastic methanogenesis. *Applied and environmental microbiology*, **60**, 467–72.

Goevert, D., & Conrad, R. (2009). Effect of substrate concentration on carbon isotope fractionation during acetoclastic methanogenesis by Methanosarcina barkeri and M. acetivorans and in rice field soil. *Applied and Environmental Microbiology*, **75**, 2605–2612. doi:10.1128/AEM.02680-08.

Gruen, D. S., Wang, D. T., Könneke, M., Topçuoğlu, B. D., Stewart, L. C., Goldhammer, T., Holden, J. F., Hinrichs, K.-U., & Ono, S. (2018). Experimental investigation on the controls of clumped isotopologue and hydrogen isotope ratios in microbial methane. *Geochimica et Cosmochimica Acta*, **237**, 339–356. doi:10.1016/J.GCA.2018.06.029.

Hattori, S., Nashimoto, H., Kimura, H., Koba, K., Yamada, K., Shimizu, M., Watanabe, H., Yoh, M., & Yoshida, N. (2012). Hydrogen and carbon isotope fractionation by thermophilic hydrogenotrophic methanogens from a deep aquifer under coculture with fermenters. *Geochemical Journal*, **46**, 193–200. doi:10.2343/geochemj.1.0161.

He, Y., Bao, H., & Liu, Y. (2019). Predicting equilibrium intramolecular isotope distribution within a large organic molecule by the cutoff calculation. *Geochimica et Cosmochimica Acta*, **269**, 292–302. doi:10.1016/j.gca.2019.10.032.

Hohenberg, P., & Kohn, W. (1964). Inhomogeneous Electron Gas. *Physical Review*, **136**, B864–B871. doi:10.1103/PhysRev.136.B864.

Holler, T., Wegener, G., Knittel, K., Boetius, A., Brunner, B., Kuypers, M. M. M., & Widdel, F. (2009). Substantial 13C/12C and D/H fractionation during anaerobic oxidation of methane by marine consortia enriched in vitro. *Environmental Microbiology Reports*, **1**, 370–376. doi:10.1111/j.1758-2229.2009.00074.x.

Horibe, Y., & Craig, H. (1995). D/H fractionation in the system methane-hydrogen-water. *Geochimica et Cosmochimica Acta*, **59**, 5209–5217. doi:10.1016/0016-7037(95)00391-6.

Horita, J. (2001). Carbon isotope exchange in the system CO2-CH4 at elevated temperatures. *Geochimica et Cosmochimica Acta*, **65**, 1907–1919. doi:10.1016/S0016-7037(01)00570-1.

Horita, J., & Wesolowski, D. J. (1994). Liquid-vapor fractionation of oxygen and hydrogen isotopes of water from the freezing to the critical temperature. *Geochimica et Cosmochimica Acta*, **58**, 3425–3437. doi:10.1016/0016-7037(94)90096-5.

Iron, M. A., & Gropp, J. (2019). Cost-Effective Density Functional Theory (DFT) Calculations of Equilibrium Isotopic Fractionation in Large Organic Molecules. *Physical Chemistry Chemical Physics*, (pp. 17555–17570). doi:10.1039/C9CP02975C.

Kaupp, M., Schleyer, P. v. R., Stoll, H., & Preuss, H. (1991). Pseudopotential approaches to Ca, Sr, and Ba hydrides. Why are some alkaline earth MX2 compounds bent? *The Journal of Chemical Physics*, **94**, 1360–1366. doi:10.1063/1.459993.

Kawagucci, S., Kobayashi, M., Hattori, S., Yamada, K., Ueno, Y., Takai, K., & Yoshida, N. (2014). Hydrogen isotope systematics among H2–H2O–CH4 during the growth of the hydrogenotrophic methanogen Methanothermobacter thermautotrophicus strain ΔH. *Geochimica et Cosmochimica Acta*, **142**, 601–614. doi:10.1016/j.gca.2014.07.020.

Kesharwani, M. K., Karton, A., & Martin, J. M. L. (2016). Benchmark ab Initio Conformational Energies for the Proteinogenic Amino Acids through Explicitly Correlated Methods. Assessment of Density Functional Methods. *Journal of chemical theory and computation*, **12**, 444–54. doi:10.1021/acs.jctc.5b01066.

Kohn, W., & Sham, L. J. (1965). Self-Consistent Equations Including Exchange and Correlation Effects. *Physical Review*, **140**, A1133–A1138. doi:10.1103/PhysRev.140.A1133.

Krzycki, J. A., Kenealy, W. R., Deniro, M. J., & Zeikus, J. G. (1987). Stable Carbon Isotope Fractionation by Methanosarcina barkeri during Methanogenesis from Acetate, Methanol, or Carbon Dioxide-Hydrogen. *Applied and environmental microbiology*, **53**, 2597–9.

Kueter, N., Schmidt, M. W., Lilley, M. D., & Bernasconi, S. M. (2019). Experimental determination of equilibrium CH4–CO2–CO carbon isotope fractionation factors (300–1200 °C). *Earth and Planetary Science Letters*, **506**, 64–75. doi:10.1016/J.EPSL.2018.10.021.

Leininger, T., Nicklass, A., Küchle, W., Stoll, H., Dolg, M., & Bergner, A. (1996). The accuracy of the pseudopotential approximation: Non-frozen-core effects for spectroscopic constants of alkali fluorides XF (X = K, Rb, Cs). *Chemical Physics Letters*, **255**, 274–280. doi:10.1016/0009-2614(96)00382-X.

Li, X., & Liu, Y. (2011). Equilibrium Se isotope fractionation parameters: A first-principles study. *Earth and Planetary Science Letters*, **304**, 113–120. doi:10.1016/J.EPSL.2011.01.022.

Liu, Q., & Liu, Y. (2016). Clumped-isotope signatures at equilibrium of CH4, NH3, H2O, H2S and SO2. *Geochimica et Cosmochimica Acta*, **175**, 252–270. doi:10.1016/J.GCA.2015.11.040.

Liu, Q., Tossell, J. A., & Liu, Y. (2010). On the proper use of the Bigeleisen–Mayer equation and corrections to it in the calculation of isotopic fractionation equilibrium constants. *Geochimica et Cosmochimica Acta*, **74**, 6965–6983. doi:10.1016/J.GCA.2010.09.014.

Londry, K. L., Dawson, K. G., Grover, H. D., Summons, R. E., & Bradley, A. S. (2008). Stable carbon isotope fractionation between substrates and products of Methanosarcina barkeri. *Organic Geochemistry*, **39**, 608–621. doi:10.1016/j.orggeochem.2008.03.002.

Marenich, A. V., Cramer, C. J., & Truhlar, D. G. (2009). Universal Solvation Model Based on Solute Electron Density and on a Continuum Model of the Solvent Defined by the Bulk Dielectric Constant and Atomic Surface Tensions. *The Journal of Physical Chemistry B*, **113**, 6378–6396. doi:10.1021/jp810292n.

McGlynn, S. E. (2017). Energy Metabolism during Anaerobic Methane Oxidation in ANME Archaea. *Microbes and environments*, **32**, 5–13. doi:10.1264/jsme2.ME16166.

Méheut, M., Lazzeri, M., Balan, E., & Mauri, F. (2007). Equilibrium isotopic fractionation in the kaolinite, quartz, water system: Prediction from first-principles density-functional theory. *Geochimica et Cosmochimica Acta*, **71**, 3170–3181. doi:10.1016/j.gca.2007.04.012.

Metz, B., Stoll, H., & Dolg, M. (2000). Small-core multiconfiguration-Dirac–Hartree–Fock-adjusted pseudopotentials for post-d main group elements: Application to PbH and PbO. *The Journal of Chemical Physics*, **113**, 2563–2569. doi:10.1063/1.1305880.

Moynier, F., & Fujii, T. (2017). Theoretical isotopic fractionation of magnesium between chlorophylls. *Scientific Reports*, **7**, 6973. doi:10.1038/s41598-017-07305-6.

Okumura, T., Kawagucci, S., Saito, Y., Matsui, Y., Takai, K., & Imachi, H. (2016). Hydrogen and carbon isotope systematics in hydrogenotrophic methanogenesis under H2-limited and H2-enriched conditions: Implications for the origin of methane and its isotopic diagnosis. *Progress in Earth and Planetary Science*, **3**, 14. doi:10.1186/s40645-016-0088-3.

Ono, S., Wang, D. T., Gruen, D. S., Sherwood Lollar, B., Zahniser, M. S., McManus, B. J., & Nelson, D. D. (2014). Measurement of a doubly substituted methane isotopologue, ^{13}CH3D, by tunable infrared laser direct absorption spectroscopy. *Analytical Chemistry*, **86**, 6487–94. doi:10.1021/ac5010579.

Otake, T., Lasaga, A. C., & Ohmoto, H. (2008). Ab initio calculations for equilibrium fractionations in multiple sulfur isotope systems. *Chemical Geology*, **249**, 357–376. doi:10.1016/J.CHEMGEO.2008.01.020.

Penger, J., Conrad, R., & Blaser, M. (2012). Stable carbon isotope fractionation by methylotrophic methanogenic archaea. *Applied and environmental microbiology*, **78**, 7596–602. doi:10.1128/AEM.01773-12.

Penger, J., Conrad, R., & Blaser, M. (2014). Stable carbon isotope fractionation of six strongly fractionating microorganisms is not affected by growth temperature under laboratory conditions. *Geochimica et Cosmochimica Acta*, **140**, 95–105. doi:10.1016/j.gca.2014.05.015.

Penning, H., Claus, P., Casper, P., & Conrad, R. (2006). Carbon isotope fractionation during acetoclastic methanogenesis by Methanosaeta concilii in culture and a lake sediment. *Applied and Environmental Microbiology*, **72**, 5648–52. doi:10.1128/AEM.00727-06.

Penning, H., Plugge, C. M., Galand, P. E., & Conrad, R. (2005). Variation of carbon isotope fractionation in hydrogenotrophic methanogenic microbial cultures and environmental samples at different energy status. *Global Change Biology*, **11**, 2103–2113. doi:10.1111/j.1365-2486.2005.01076.x.

Proskurowski, G., Lilley, M. D., Kelley, D. S., & Olson, E. J. (2006). Low temperature volatile production at the Lost City Hydrothermal Field, evidence from a hydrogen stable isotope geothermometer. *Chemical Geology*, **229**, 331–343. doi:10.1016/J.CHEMGEO.2005.11.005.

Richet, P., Bottinga, Y., & Javoy, M. (1977). A Review of Hydrogen, Carbon, Nitrogen, Oxygen, Sulphur, and Chlorine Stable Isotope Fractionation Among Gaseous Molecules. *Annual Review of Earth and Planetary Sciences*, **5**, 65–110. doi:10.1146/annurev.ea.05.050177.000433.

Rolston, J. H., Den Hartog, J., & Butler, J. P. (1976). The deuterium isotope separation factor between hydrogen and liquid water. *The Journal of Physical Chemistry*, **80**, 1064–1067. doi:10.1021/j100551a008.

Roothaan, C. C. J. (1951). New Developments in Molecular Orbital Theory. *Reviews of Modern Physics*, **23**, 69–89. doi:10.1103/RevModPhys.23.69.

Rosenfeld, W. D., & Silverman, S. R. (1959). Carbon Isotope Fractionation in Bacterial Production of Methane. *Science*, **130**, 1658–1659. doi:10.1126/science.130.3389.1658-a.

Rustad, J. R. (2009). Ab initio calculation of the carbon isotope signatures of amino acids. *Organic Geochemistry*, **40**, 720–723. doi:10.1016/j.orggeochem.2009.03.003.

Rustad, J. R., Nelmes, S. L., Jackson, V. E., & Dixon, D. A. (2008). Quantum-chemical calculations of carbon-isotope fractionation in CO2(g), aqueous carbonate species, and carbonate minerals. *The journal of physical chemistry. A*, **112**, 542–55. doi:10.1021/jp076103m.

Scheller, S., Ermler, U., & Shima, S. (2017). Catabolic Pathways and Enzymes Involved in Anaerobic Methane Oxidation. In *Anaerobic Utilization of Hydrocarbons, Oils, and Lipids* (pp. 1–29). Springer International Publishing. doi:10.1007/978-3-319-33598-8-3-1.

Scheller, S., Goenrich, M., Boecher, R., Thauer, R. K., & Jaun, B. (2010). The key nickel enzyme of methanogenesis catalyses the anaerobic oxidation of methane. *Nature*, **465**, 606–8. doi:10.1038/nature09015.

Scheller, S., Goenrich, M., Thauer, R. K., & Jaun, B. (2013). Methyl-coenzyme M reductase from methanogenic archaea: Isotope effects on the formation and anaerobic oxidation of methane. *Journal of the American Chemical Society*, **135**, 14975–84. doi:10.1021/ja406485z.

Stolper, D., Lawson, M., Davis, C. L., Ferreira, A. A., Santos Neto, E. V., Ellis, G. S., Lewan, M. D., Martini, A. M., Tang, Y., Schoell, M., Sessions, A. L., & Eiler, J. M. (2014). Formation temperatures of thermogenic and biogenic methane. *Science*, **344**, 1500–1503. doi:10.1126/science.1254509.

Stolper, D., Martini, A., Clog, M., Douglas, P., Shusta, S., Valentine, D., Sessions, A., & Eiler, J. (2015). Distinguishing and understanding thermogenic and biogenic sources of methane using multiply substituted isotopologues. *Geochimica et Cosmochimica Acta*, **161**, 219–247. doi:10.1016/j.gca.2015.04.015.

Suess, H. E. (1949). Das Gleichgewicht H2 + HDO = HD + H2O und die weiteren Austauschgleichgewichte im System H2 , D2 und H2O. *Zeitschrift für Naturforschung A*, **4**, 328–332. doi:10.1515/ZNA-1949-0502.

Takai, K., Nakamura, K., Toki, T., Tsunogai, U., Miyazaki, M., Miyazaki, J., Hirayama, H., Nakagawa, S., Nunoura, T., & Horikoshi, K. (2008). Cell proliferation at 122 degrees C and isotopically heavy CH4 production by a hyperthermophilic methanogen under high-pressure cultivation. *Proceedings of the National Academy of Sciences of the United States of America*, **105**, 10949–54. doi:10.1073/pnas.0712334105.

Tennant, A., Rauk, A., & Wieser, M. E. (2017). Computational modelling of the redistribution of copper isotopes by proteins in the liver. *Metallomics*, **9**, 1809–1819. doi:10.1039/C7MT00248C.

Thauer, R. K. (2011). Anaerobic oxidation of methane with sulfate: On the reversibility of the reactions that are catalyzed by enzymes also involved in methanogenesis from CO2. *Current Opinion in Microbiology*, **14**, 292–299. doi:10.1016/j.mib.2011.03.003.

Thauer, R. K., Kaster, A.-K., Seedorf, H., Buckel, W., & Hedderich, R. (2008). Methanogenic archaea: Ecologically relevant differences in energy conservation. *Nature reviews. Microbiology*, **6**, 579–591. doi:10.1038/nrmicro1931.

Tomasi, J., Mennucci, B., & Cammi, R. (2005). Quantum Mechanical Continuum Solvation Models. *Chemical Reviews*, **105**, 2999–3093. doi:10.1021/cr9904009.

Topçuoğlu, B. D., Meydan, C., Nguyen, T. B., Lang, S. Q., & Holden, J. F. (2019). Growth Kinetics, Carbon Isotope Fractionation, and Gene Expression in the Hyperthermophile Methanocaldococcus jannaschii during Hydrogen-Limited Growth and Interspecies Hydrogen Transfer. *Applied and Environmental Microbiology*, **85**, 1–14. doi:10.1128/AEM.00180-19.

Urey, H. C. (1947). The thermodynamic properties of isotopic substances. *Journal of the Chemical Society (Resumed)*, (pp. 562–581). doi:10.1039/jr9470000562.

Valentine, D. L., Chidthaisong, A., Rice, A., Reeburgh, W. S., & Tyler, S. C. (2004). Carbon and hydrogen isotope fractionation by moderately thermophilic methanogens. *Geochimica et Cosmochimica Acta*, **68**, 1571–1590. doi:10.1016/j.gca.2003.10.012.

Vanwonterghem, I., Evans, P. N., Parks, D. H., Jensen, P. D., Woodcroft, B. J., Hugenholtz, P., & Tyson, G. W. (2016). Methylotrophic methanogenesis discovered in the archaeal phylum Verstraetearchaeota. *Nature Microbiology*, **1**, 16170. doi:10.1038/nmicrobiol.2016.170.

Wang, D. T., Gruen, D. S., Lollar, B. S., Hinrichs, K.-U., Stewart, L. C., Holden, J. F., Hristov, A. N., Pohlman, J. W., Morrill, P. L., Könneke, M., Delwiche, K. B., Reeves, E. P., Sutcliffe, C. N., Ritter, D. J., Seewald, J. S., McIntosh, J. C., Hemond, H. F., Kubo, M. D., Cardace, D., Hoehler, T. M., & Ono, S. (2015). Nonequilibrium clumped isotope signals in microbial methane. *Science*, **348**, 428–431. doi:10.1126/science.aaa4326.

Wang, D. T., Reeves, E. P., McDermott, J. M., Seewald, J. S., & Ono, S. (2017). Clumped isotopologue constraints on the origin of methane at seafloor hot springs. *Geochimica et Cosmochimica Acta*, **223**, 141–158. doi:10.1016/j.gca.2017.11.030.

Wang, Y., Sessions, A. L., Nielsen, R. J., & Goddard, W. A. (2009a). Equilibrium 2H/1H fractionations in organic molecules: I. Experimental calibration of ab initio calculations. *Geochimica et Cosmochimica Acta*, **73**, 7060–7075. doi:10.1016/J.GCA.2009.08.019.

Wang, Y., Sessions, A. L., Nielsen, R. J., & Goddard, W. A. (2009b). Equilibrium 2H/1H fractionations in organic molecules. II: Linear alkanes, alkenes, ketones, carboxylic acids, esters, alcohols and ethers. *Geochimica et Cosmochimica Acta*, **73**, 7076–7086. doi:10.1016/J.GCA.2009.08.018.

Wang, Y., Sessions, A. L., Nielsen, R. J., & Goddard, W. A. (2013). Equilibrium 2H/1H fractionation in organic molecules: III. Cyclic ketones and hydrocarbons. *Geochimica et Cosmochimica Acta*, **107**, 82–95. doi:10.1016/J.GCA.2013.01.001.

Webb, M. A., & Miller, T. F. (2014). Position-specific and clumped stable isotope studies: Comparison of the Urey and path-integral approaches for carbon dioxide, nitrous oxide, methane, and propane. *The journal of physical chemistry. A*, **118**, 467–74. doi:10.1021/jp411134v.

Weigend, F., & Ahlrichs, R. (2005). Balanced basis sets of split valence, triple zeta valence and quadruple zeta valence quality for H to Rn: Design and assessment of accuracy. *Physical Chemistry Chemical Physics*, **7**, 3297. doi:10.1039/b508541a.

Welte, C., & Deppenmeier, U. (2014). Bioenergetics and anaerobic respiratory chains of aceticlastic methanogens. *Biochimica et Biophysica Acta (BBA) - Bioenergetics*, **1837**, 1130–1147. doi:10.1016/J.BBABIO.2013.12.002.

Wenk, C. B., Wing, B. A., & Halevy, I. (2017). Electron carriers in microbial sulfate reduction inferred from experimental and environmental sulfur isotope fractionations. *The ISME Journal*, **12**, 495–507. doi:10.1038/ismej.2017.185.

Whiticar, M. J. (1999). Carbon and hydrogen isotope systematics of bacterial formation and oxidation of methane. *Chemical Geology*, **161**, 291–314. doi:10.1016/S0009-2541(99)00092-3.

Wing, B. A., & Halevy, I. (2014). Intracellular metabolite levels shape sulfur isotope fractionation during microbial sulfate respiration. *Proceedings of the National Academy of Sciences of the United States of America*, **111**, 18116–25. doi:10.1073/pnas.1407502111.

Yoshinaga, M. Y., Holler, T., Goldhammer, T., Wegener, G., Pohlman, J. W., Brunner, B., Kuypers, M. M. M., Hinrichs, K.-U., & Elvert, M. (2014). Carbon isotope equilibration during sulphate-limited anaerobic oxidation of methane. *Nature Geoscience*, **7**, 190–194. doi:10.1038/ngeo2069.

Yoshioka, H., Sakata, S., & Kamagata, Y. (2008). Hydrogen isotope fractionation by Methanothermobacter thermoautotrophicus in coculture and pure culture conditions. *Geochimica et Cosmochimica Acta*, **72**, 2687–2694. doi:10.1016/j.gca.2008.03.015.

Young, E. D. (2019). A Two-Dimensional Perspective on CH4 Isotope Clumping. In *Deep Carbon: Past to Present* (pp. 388–414). Cambridge University Press.

Zaarur, S., Wang, D. T., Ono, S., & Bosak, T. (2017). Influence of Phosphorus and Cell Geometry on the Fractionation of Sulfur Isotopes by Several Species of Desulfovibrio during Microbial Sulfate Reduction. *Frontiers in Microbiology*, **8**, 890. doi:10.3389/fmicb.2017.00890.

Zhao, Y., Schultz, N. E., & Truhlar, D. G. (2006). Design of Density Functionals by Combining the Method of Constraint Satisfaction with Parametrization for Thermochemistry, Thermochemical Kinetics, and Noncovalent Interactions. *Journal of Chemical Theory and Computation*, **2**, 364–382. doi:10.1021/ct0502763.

Zhuang, G.-C., Heuer, V. B., Lazar, C. S., Goldhammer, T., Wendt, J., Samarkin, V. A., Elvert, M., Teske, A. P., Joye, S. B., & Hinrichs, K.-U. (2018). Relative importance of methylotrophic methanogenesis in sediments of the Western Mediterranean Sea. *Geochimica et Cosmochimica Acta*, **224**, 171–186. doi:10.1016/j.gca.2017.12.024.